MICROWAVE LABORATORY REPORT NO. 89-P-3

A STUDY OF A NEW TIME-DOMAIN METHOD OF LINES AND ITS

APPLICATION FOR THE CHARACTERIZATION OF MICROSTRIP

LINE AND ITS DISCONTINUITIES

TECHNICAL REPORT

SANGWOOK NAM, HAO LING AND TATSUO ITOH

Accession For	
NTIS GRA&I	☒
DTIC TAB	☐
Unannounced	☐
Justification	
By	
Distribution/	
Availability Codes	
Dist	Avail and/or Special
A-1	

MAY 1989

THE UNIVERSITY OF TEXAS

DEPARTMENT OF ELECTRICAL ENGINEERING

AUSTIN, TEXAS 78712

SECURITY CLASSIFICATION OF THIS PAGE (When Data Entered)

REPORT DOCUMENTATION PAGE		READ INSTRUCTIONS BEFORE COMPLETING FORM
1. REPORT NUMBER	2. GOVT ACCESSION NO.	3. RECIPIENT'S CATALOG NUMBER
4. TITLE (and Subtitle) A Study of a New Time-Domain Method of Lines and Its Application for the Characterization of Microstrip Line and Its Discontinuities		5. TYPE OF REPORT & PERIOD COVERED Technical Report
		6. PERFORMING ORG. REPORT NUMBER 89-P-3
7. AUTHOR(s) Sangwook Nam, Hao Ling and Tatsuo Itoh		8. CONTRACT OR GRANT NUMBER(s) N00014-89-J-1006
9. PERFORMING ORGANIZATION NAME AND ADDRESS Dept. of Electrical & Computer Engineering The University of Texas Austin, TX 78712		10. PROGRAM ELEMENT, PROJECT, TASK AREA & WORK UNIT NUMBERS
11. CONTROLLING OFFICE NAME AND ADDRESS		12. REPORT DATE May 1989
		13. NUMBER OF PAGES 100
14. MONITORING AGENCY NAME & ADDRESS(if different from Controlling Office)		15. SECURITY CLASS. (of this report)
		15a. DECLASSIFICATION/DOWNGRADING SCHEDULE

16. DISTRIBUTION STATEMENT (of this Report)

17. DISTRIBUTION STATEMENT (of the abstract entered in Block 20, if different from Report)

18. SUPPLEMENTARY NOTES

19. KEY WORDS (Continue on reverse side if necessary and identify by block number)

Time-Domain Method, Microstrip Line, Method of Lines

20. ABSTRACT (Continue on reverse side if necessary and identify by block number)

A new time-domain method for the analysis fo planar guided wave propagation and scattering is developed in which an analytical process is incorporated along one of the spatial dimensions. The method makes use of the Method of Lines which has been applied to microwave problems in the time-harmonic cases.

DD FORM 1473 EDITION OF 1 NOV 65 IS OBSOLETE
1 JAN 73
S/N 0102-014-6601 1

SECURITY CLASSIFICATION OF THIS PAGE (When Data Entered)

Abstract

A new time-domain method for the analysis of planar guided wave propagation and scattering is developed in which an analytical process is incoporated along one of the spatial dimensions. The method makes use of the Method of Lines which has been applied to microwave problems in the time-harmonic cases.

The procedure and the formulation of the proposed method to calculate the time history of a pulse scattered in a partially filled waveguide and a finned waveguide are described in detail. The cutoff characteristics of the structures can be derived via the Fourier transform of the time-domain pulse scattering data. The results are compared with other available data.

The method is extended to characterize three-dimensional structures. The procedure and the formulation of the three-dimensional analysis are explained. The propagation and scattering data of a pulse in a planar transmission line with its discontinuities can be obtained by using the three-dimensional analysis. From the time-domain data, the frequency-domain characteristics for a wide range of frequencies can be extracted by the Fourier transform. The important design parameters such as the characteristic impedance and the propagation constant of a uniform microstrip line and the scattering parameters of its discontinuities (step-in-width, open-end and gap discontinuities) are presented and con.. with available published data.

TABLE OF CONTENTS

Chapter 1

Introduction

1.1. Background and Goals of This Dissertation

A discontinuity in a planar transmission line circuit is caused by an abrupt change in the geometry of the strip conductor, as shown in Fig. 1.1. Therefore, electric and magnetic field distributions are modified near this discontinuity. At low frequencies, the discontinuity dimensions are much smaller than the wavelength. In this case, the altered electric and magnetic field distribution can be approximated by lumped element equivalent circuits. However, as the operating frequency increases, accurate frequency-dependent scattering matrix representations associated with discontinuities are necessary for a accurate design of a microwave and millimeter-wave circuit. Especially, the present cut-and-try cycles in the Microwave Integrated Circuit (MIC) / Monolithic Millimeter-Wave Integrated Circuit (MMIC) will be greatly reduced if the accurate frequency-dependent characteristics of discontinuity can be obtained.

In the early stages of the study of discontinuities, analyses were mostly done by quasi-static methods [1~10]. In all these methods, the following assumptions are implied: (i) the size of the discontinuity is small compared with the wavelength so that the phase variation across the discontinuity can be neglected, (ii) the current on the strip has no divergence and (iii) the strip conductor is infinitely thin.

1
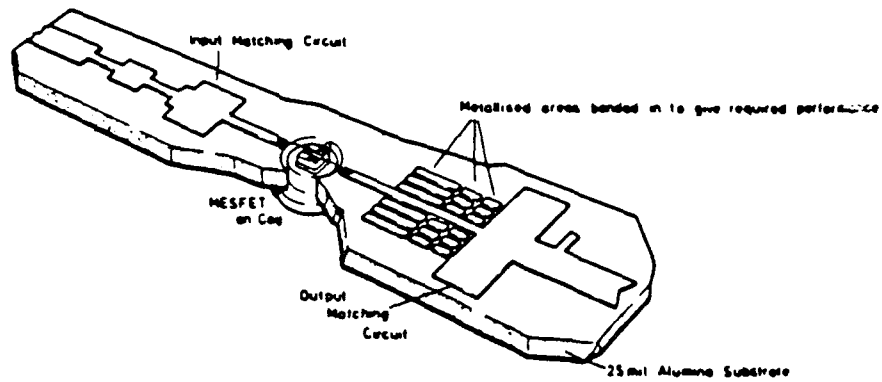
Fig. 1.1(a) The layout of a microwave amplifier using a gallium arsennide MESFET device, showing discontinuities in the microstrip lines.

(i)   (ii)

(iii)

(iv)   (v)   (vi)
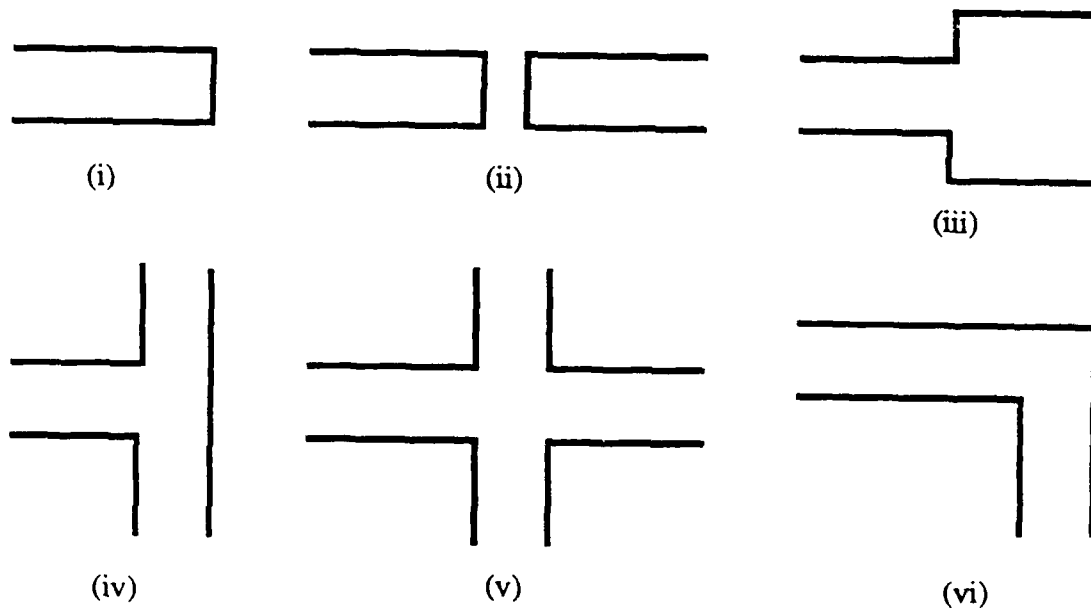
Fig. 1.1(b) Various microstrip discontinuities appearing in microwave integrated circuits. (i) open-end, (ii) gap, (iii) step-in-width, (iv) T-junction, (v) cross-junction and (vi) bend

Because of these assumptions, quasi-static analysis is valid only up to a few gigahertz. Therefore, fullwave analysis is required to determine the frequency-dependence of various parameters needed for a complete characterization of the discontinuity. The first fullwave analysis was done by using a planar waveguide model [11,12], where the frequency dependent scattering parameters can be obtained by matching the field in each waveguide at the discontinuity interface using the planar waveguide model. The Spectral Domain Method / Transverse Resonance Technique can also be used to obtain the frequency-dependent scattering parameters for various discontinuities [13~16]. More recently, the moment method has been used by several investigators to characterize discontinuities, where radiation and surface wave effects can be included [17,18].

All of the above mentioned approaches have been performed in the frequency domain; that is, the data for the whole frequency range are calculated one frequency at a time. This is an expensive approach when the results over a wide frequency range are sought. Since a pulse response contains all the information of a system for the whole frequency range, it is natural to use a pulse to excite a planar circuit in a time-domain approach. From the time-domain pulse response, the frequency-domain characteristics of the structure can be extracted via the Fourier transform. Therefore, the time-domain analysis of microwave planar transmission structures provides an alternative to time-harmonic approaches, and it is also useful for studying the behavior of pulsed signal in such structures as high speed digital circuits. The knowledge of time-domain propagation and scattering can be used for circuit diagnosis by means of a fast pulse.

A typical time-domain analysis requires a discretization of the three-dimensional space into the three-dimensional mesh, as shown in Fig. 1.2. Maxwell's

$t = N\Delta t$ $t = (N+1)\Delta t$

(a)

$t = N\Delta t$ $t = (N+1/2)\Delta t$

(b)
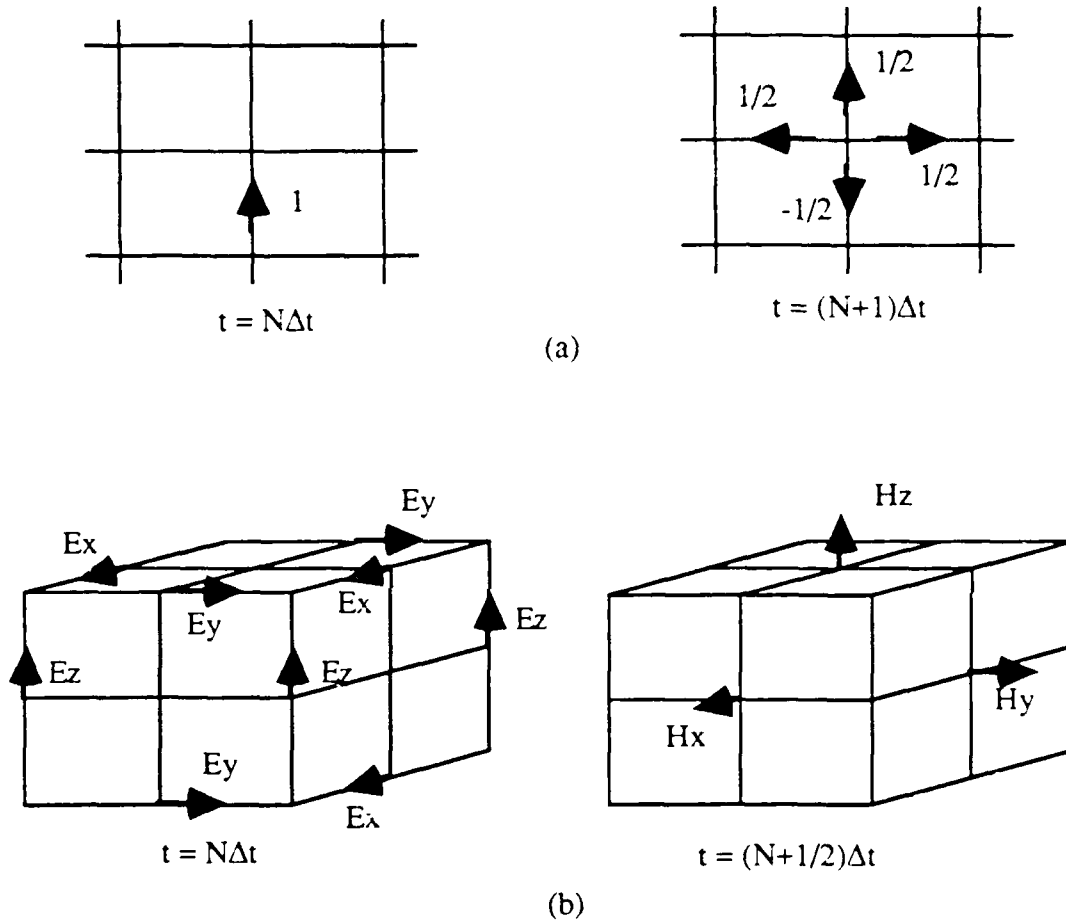
Fig. 1.2. Examples of the discretization scheme in (a) TLM method in two-dimensional plane, and (b) FDTD in three-dimensional space.

equations can be discretized at these points, as in the case of Finite-Difference Time-Domain method (FDTD) [19], or the wave phenomena can be modeled by networks, as in the case of the Transmission Line Matrix (TLM) method [20] and the Bergeron's

method [21] These techniques have been applied by several investigators to microwave planar transmission lines in order to study the time-domain pulse propagation and scattering phenomena, and the frequency-domain data have been derived from the time-domain information. In [22] and [23], Bergeron's method was used to obtain the qualitative results that graphically illustrate the pulse propagation and coupling in the microstrip-bend and the crossing. In [24], the TLM method was used to obtain some characteristics of fin lines. In [25] and [26], the FDTD method has been used to obtain the behavior of a pulsed signal along a uniform microstrip line with various discontinuities, from which the frequency-dependent design information for the uniform microstrip line and its discontinuities was extracted. Usually, large amount of computer storage and long computation time are

(a)   (b)

(c)   (d)
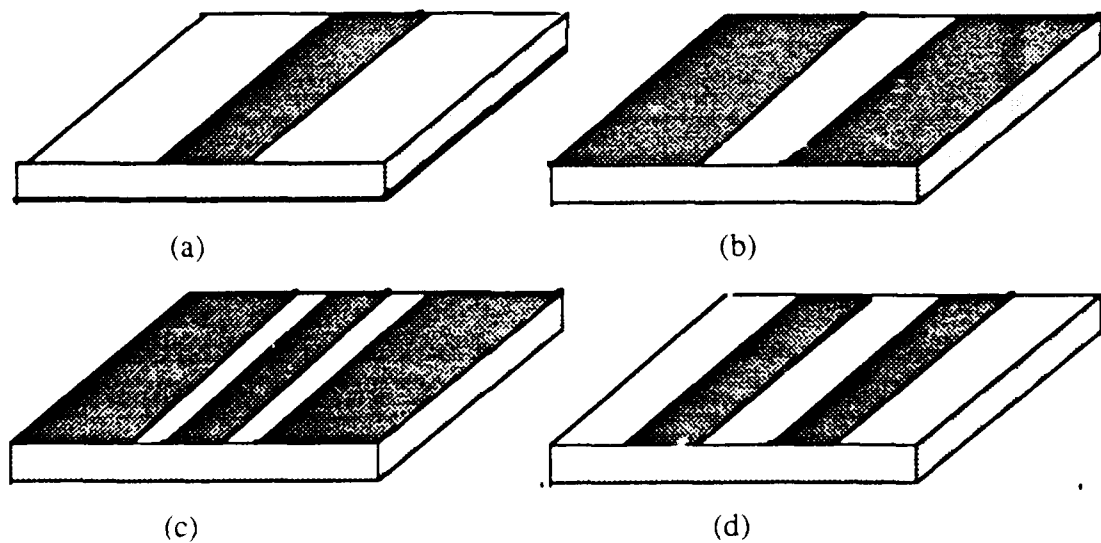
Fig. 1.3. Several planar transmission lines used in MICs. (a) microstrip, (b) slotline, (c) coplanar waveguide, and (d) coplanar strip.

required for these aforementioned time-domain analyses. An additional problem of these methods is the difficulty in handling open boundaries.

In this study, a new time-domain method is proposed, that originates from the fact that most of the discontinuities in the planar transmission structure are located on the substrate surface, and the space above and below this surface is uniform and homogeneous as shown in Fig. 1.3. One wants to make use of this structural feature and wishes to solve the problem by discretizing the structure in only the two-dimensional surface on the substrate instead of using the conventional three-dimensional discretization. This is possible if the wave scattering phenomena in the direction normal to the substrate surface can be derived analytically By using an analytical solution in one direction, the dimension of the problem is effectively reduced by one so that computer storage and computation time may be saved. The present method actually incoporates this process and is essentially an extention of the frequency-domain analysis called the Method of Lines.

The Method of Lines technique was developed by mathematicians in order to solve partial differential equations[27]. The Method of Lines is simple in concept: for a given system of partial differential equations, all but one of the independent variables are discretized to obtain a system of ordinary differential equations so that the whole space is represented by a number of lines. This semi-analytical procedure is apparently very useful in the calculation of planar transmission structures. This is because these structures consist of regions, which are homogeneous in one direction as shown in Fig. 1.3. Moreover, this method has no problem with so called "relative convergence" phenomenon sometimes encountered in mode-matching and Galerkin's method.

The application of Method of Lines in microwave field analysis was first introduced in [28] for the calculation of the propagation constant and the characteristic impedance of microstrip lines. The method has also been extended to three dimensional problems such as the calculation of the resonant frequencies of an arbitrarily shaped planar resonator [29]. There have also been several publications in which the Method of Lines was modified for the analysis of a quasi-planar structure or for better performance [30]. Those papers, however, have always used the Method of Lines to solve time-harmonic Maxwell's equations.

This study describes a new time-domain method termed Time-Domain Method of Lines (TDML). The goals of this dissertation are as follows.

(1) Development of the procedure and formulation of the new method.

(2) Verification of the method by solving several simple two-dimensional problems and comparing the results with those obtained by other methods.

(3) Application of the new method to three-dimensional structures to obtain useful design data.

1.2 Dissertation Organization

Following Chapter 1, Chapter 2 presents the basic discrete mathematics related to the Method of Lines - boundary condition, discretization scheme, difference operators and diagonalization matrix. In Chapter 3, the analysis of the two-dimensional structure with a uniform interface boundary condition is formulated and the behavior of an initial pulse inside the partially filled rectangular waveguide is investigated using the present method. The cutoff frequency spectrum of the structure is obtained via the Fourier transform of the time-domain data. In Chapter 4, the

procedure developed in Chapter 3 is modified to deal with problems where the metalization exists on the substrate surface. In this situation, a non-uniform interface boundary condition results. The procedure is used to calculate the cutoff frequency spectrum of a finned waveguide by the Fourier transform of the time-domain data. In Chapter 5, the formulation of the Time-Domain Method of Lines for the characterization of the wave propagation and scattering property in the three-dimensional problems is described in detail. The results of the time-domain data and the derived frequency-domain characteristics for the uniform microstrip line and its discontinuities (step-in-width, open-end and gap discontinuities) are presented. Chapter 6 summarizes the contributions of this study and proposes some related problems for future research.

Chapter 2
Preliminary

2.1. Outline of the Proposed Method

As pointed out in Chapter 1, the proposed method originates from the fact that most of the discontinuites appearing in the planar transmission line structures are located on the substrate surface, and the space below and above this surface is uniform and homogeneous. One wants to use this structural feature and wishes to solve the problem by discretizing the space only in the two-dimensional surface on the substrate where the discontinuity is located. This is possible if the wave-scattering information in the direction perpendicular to the substrate surface is available analytically. The new method actually incorporates this process and entails discretization of the structure by a number of lines perpendicular to substrate surface as shown in Fig 2.1. At a specified time, the field distribution at each intersection of these lines with the substrate surface is calculated by Maxwell's equations discretized only in the x and z directions parallel to the substrate surface. The field information in the y direction is obtained analytically at each point and time. This information can be found from the inverse spatial transform of the solution of the frequency-domain Helmholtz equation in the y direction.

One may wonder as to what is happening to the wave scattering phenomena that are taking place everywhere in the waveguide, not only on the substrate surface.
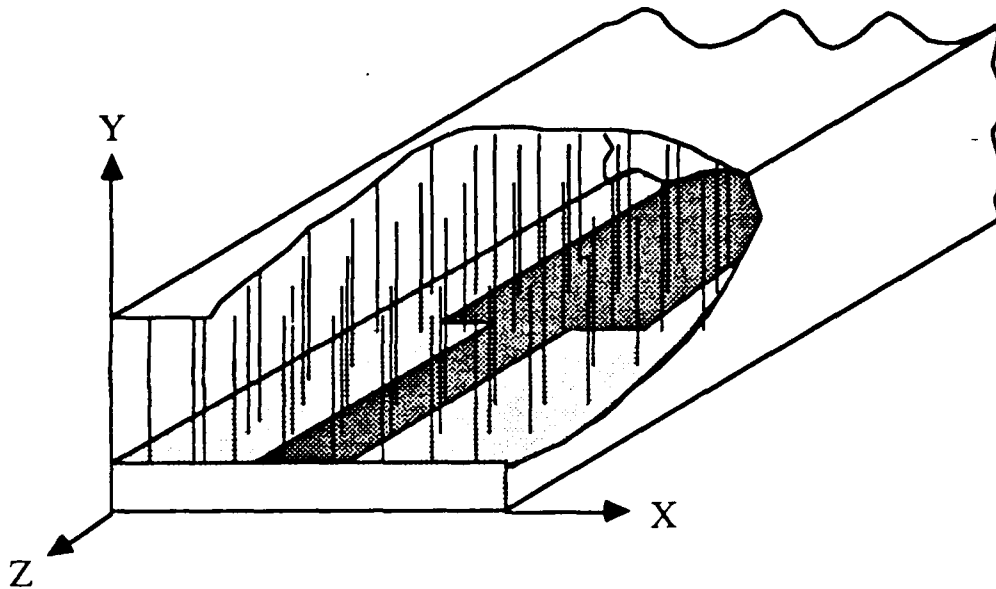
Fig. 2.1. The discretization scheme of the method of lines. The three-dimensional

space is discretized by a collection of lines parallel to the y-axis.

This question is natural, because in other time-domain methods the electromagnetic

fields at one mesh point interact with those at all six neighboring mesh points in the x,

y, and z directions. In the proposed method, the fields at any point on one

discretization line do not appear to interact with those on a similar point on another

line. It should be emphasized that this is not the case. As will be seen in the

formulation, a spatial transformation is introduced by which the field as a function of

(discretized) x and z is transformed to another discretized quantity which contains the

field quantities at all x and z values. The analytical information in the y direction is

then applied to this transformed quantity. Since analytical expressions are used for

the field variation in the y direction, this method can easily handle the case where the

top wall is removed and the structure is open in the y direction.

2.2. Discrete Mathematics Related to the Method of Lines

As explained above, the proposed method is a "semi-analytical method" for solving the time-dependent Maxwell's equation in a planar waveguide structure so that the discrete expressions as well as the analytical expressions need to be used in the formulation. Therefore, it is important to become farmilar with some discrete mathematics related to the method of lines before the formulation of the method is explained. This mathematics will be used to derive all the formulations described in later chapters.

2.2.1. Lateral Boundary Conditions and Discretization Scheme

Let ϕ be a field component of interest. The boundary condition for ϕ is always given by either the Dirichlet or the Neumann condition because the circuit to be considered in this study is always enclosed by perfect electric walls. Since all the space variables (x and z) except one (y) are discretized in the Method of Lines, the original continuous space is approximated by a number of lines parallel to the y-axis located only at discretized positions in x-z plane, as shown in Fig. 2.1. The locations of these discretized points are determined by the boundary condition of the field component, ϕ. For example, if a boundary is known to be a Dirichlet-boundary to ϕ, the position of the first discretization point for ϕ is $\Delta\xi$ away from the boundary where $\Delta\xi$ is the unit discretization length in ξ direction. On the other hand, if the boundary is a Neumann-boundary, the first discretization position is $\Delta\xi/2$ away from the boundary. Figure 2.2 shows the difference of the discretization scheme between the Dirichlet-boundary and Neumann-boundary . One thing to be noticed here is that the two set of the discretization points are shifted by $\Delta\xi/2$. This discretization scheme

reduces the discretization error and makes the second-order difference operator symmetric [28].

$\phi = 0$ $\delta\phi/\delta\xi = 0$

(a)   image lines   (b)
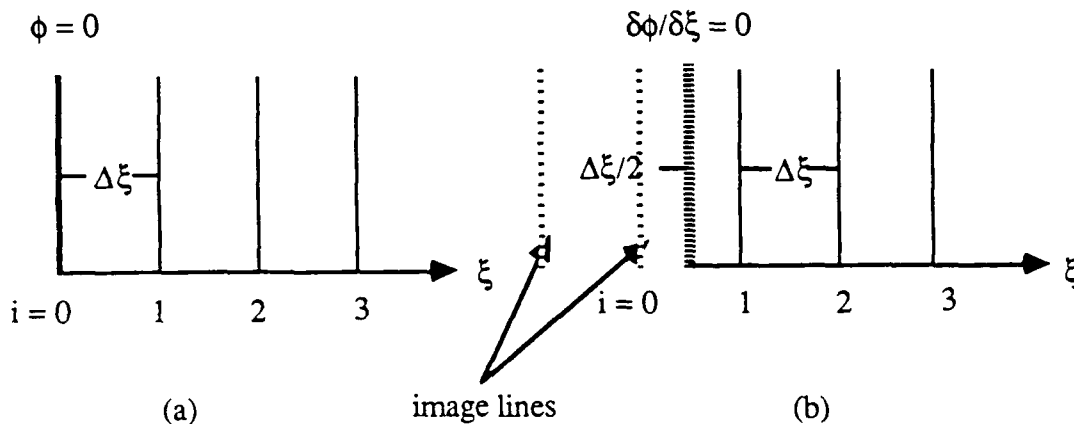
Fig. 2.2. Different discretization schemes corresponding to the boundary conditions.

(a) Dirichlet-boundary, (b) Neumann-boundary.

Figure 2.3 shows the outer boundary of two typical structures to be considered in this dissertation. One is a rectangular waveguide for the two-dimensional problem and the other is a rectangular waveguide resonator for the three-dimensional problem. The waveguide walls consist of perfect electric walls so that the lateral boundary condition for ϕ along any axis is always given by either the Dirichlet or Neumann boundary condition. Since there always exist two boundaries along one axis, there are four combinations of the lateral boundary condition in one direction. Figure 2.4 shows the diagrams of these combinations and the appropriate discretization positions for each case, in which the axis is assumed to be x.
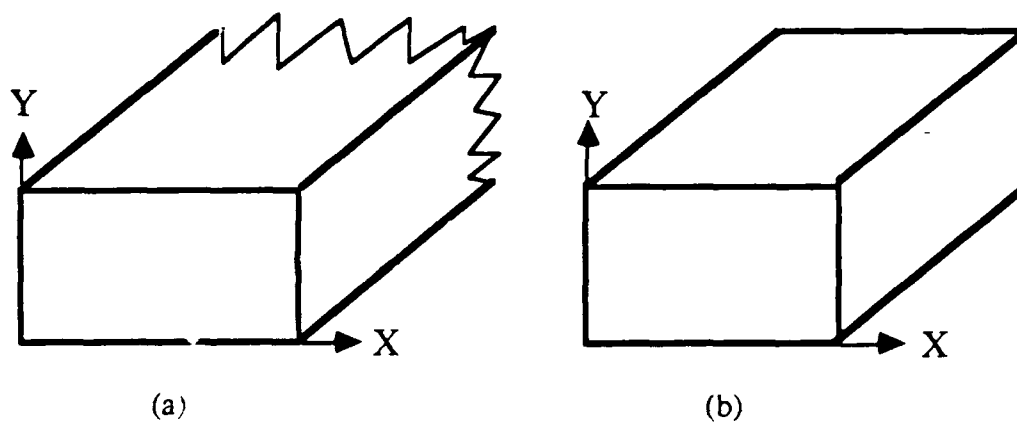
Fig. 2.3. The outer boundary of the structures considered in this study.

(a) rectangular waveguide, (b) rectangular waveguide resonator.
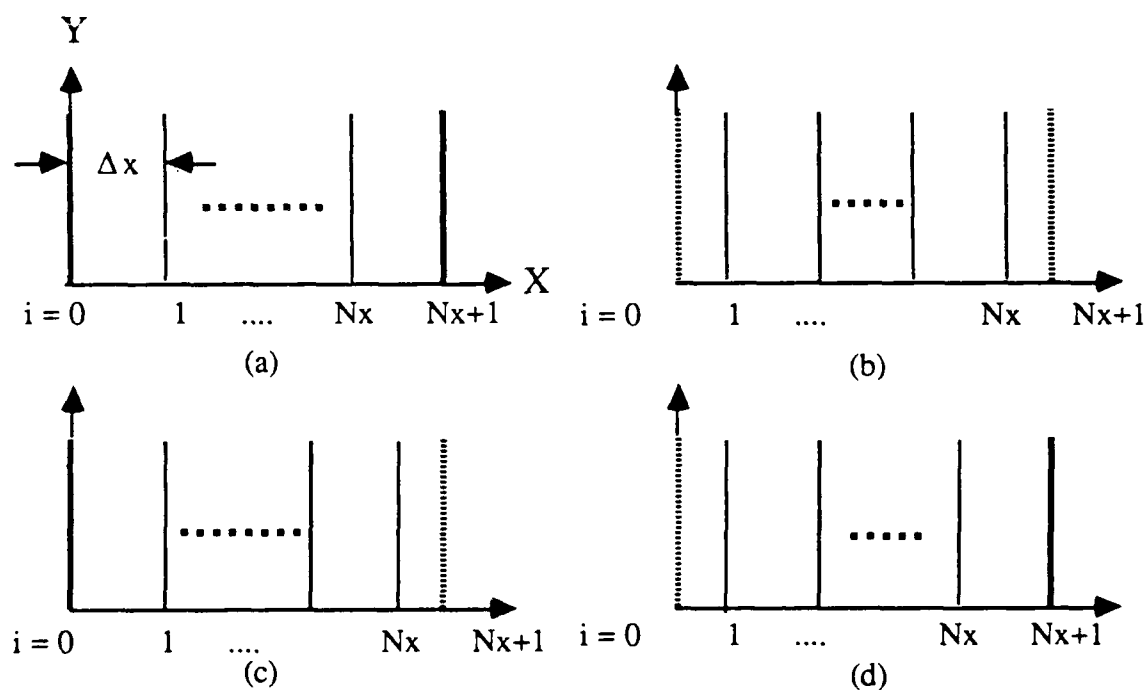
Fig. 2.4. Four cases of lateral boundary condition combination.

(a) D-D, (b) N-N, (c) D-N, and (d) N-D.

So far, only the one-dimensional (along the x-axis) discretization scheme has been discussed. However, the two-dimensional discretization (in the x-z plane) is required to solve the three-dimensional problem. In that case, both the x- and the z-direction are discretized independently according to the discretization scheme discribed above. A typical two-dimensional discretization example is shown in Fig. 2.5 where the N-D boundary condition is assumed along both the x-direction and the z-direction.
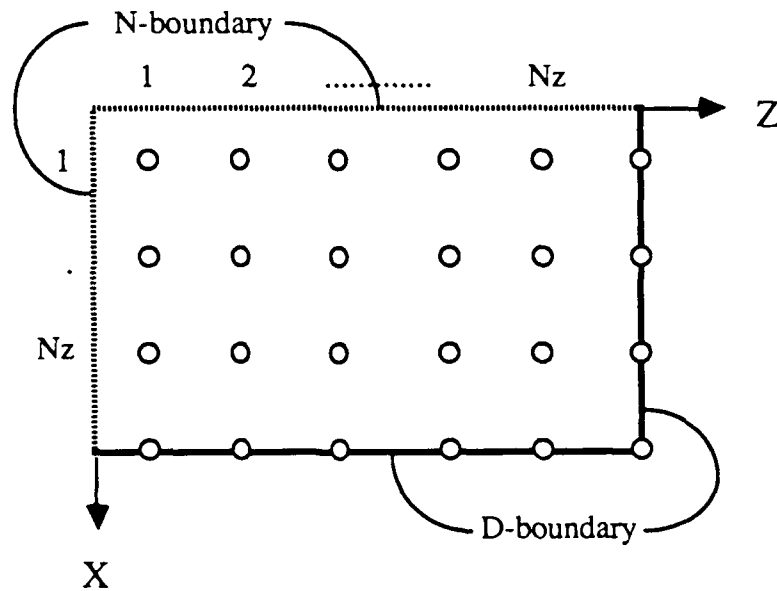

Fig. 2.5. A two-dimensional discretization example where N-D boundary condition is assumed along the x- and the z-axis.

2.2.2. Matrix Operators

In addition to the discretization of the space according to the boundary condition of the field, the derivatives of the field with respect to the discretized variable should be modified to a discrete form. In this section, the difference

operators are introduced as a discrete form of a derivative, and the relation between them will be derived.

2.2.2.1. First-Order Difference Operator

After the discretization of the space using the discretization scheme discribed in Section 2.2.1, the original field defined in the continuous whole region can be approximated by a collection of constituent field lines, $\phi_i(y)$, defined only at the discretized position i. In the cases of Fig. 2.4,

$$\phi(x,y) \longrightarrow [\phi_i(y)]^t = [\phi_1, \phi_2, \dots, \phi_N]^t \qquad (2.1)$$

where the i-th element represents the field of the i-th line.

Accordingly, the derivative with respect to the discretized variable, x, is replaced by the difference operation of two consecutive lines using the central difference scheme. That is,

$$\partial\phi(x,y) / \partial x \longrightarrow \partial\phi / \partial x \mid_i = [\phi_i - \phi_{i-1}] / \Delta x \quad \text{for i = 1 to N+1} \qquad (2.2)$$

which can be represented in terms of the matrix.

$$\Delta x \frac{\partial\phi(x,y)}{\partial x} \longrightarrow
\begin{bmatrix}
-1 & 1 & & & \\
 & -1 & 1 & & 0 \\
 & & \cdot & \cdot & \\
 & & & \cdot & \cdot \\
 0 & & & & \\
 & & & & -1 & 1
\end{bmatrix}
\begin{bmatrix}
\phi_0 \\
\phi_1 \\
\vdots \\
\vdots \\
\phi_N \\
\phi_{N+1}
\end{bmatrix}
= [D_x][\phi_i] \qquad (2.3)$$

where $[D_x]$ is a matrix that acts as a difference operator with respect to x.

boundary\condition	Dirichlet	Neumann
left boundary	$\phi_0 = 0$	$\phi_0 = \phi_1$
right boundary	$\phi_{N+1} = 0$	$\phi_N = \phi_{N+1}$

Table 2.1. Boundary conditions represented by the field values near the boundary.

The specific forms of the difference operator, which include the lateral boundary conditions, can be derived by imposing the appropriate conditions (see Table 2.1) on equation (2.3). The resulting first-order difference operators are summarized in Table 2.2. Although the operators shown in Table 2.2 are derived from the derivative with respect to x, they can also be used for derivatives with respect to the other variables. From table 2.2, it is easy to find the relationship between the operators which will be used in the later formulation.

$$[D^{ND}] = - [D^{DN}]^t \qquad\qquad (2.4)$$

$$[D^{NN}] = - [D^{DD}]^t \qquad\qquad (2.5)$$

where the superscripts ND,DN,NN,and DD represent the specific lateral boundary conditions(left-right) associated with the difference operator, and the superscript t represents the transpose of the matrix.

One thing to be noticed here is that the values of the derivative obtained from the difference operation are defined only at the mid-point between two consecutive

points (i.e. the central difference). That is, the actual position of the i-th line of $\partial\phi$ / ∂x is at the center of the i- and (i+1)-th positions of ϕ in the equation (2.2).

boundary conditions (left - right)	[D]	[d]	elements of [d]
N-D	$\begin{bmatrix} -1 & 1 & & \\ & & \ddots & \\ & & & 1 \\ & & & -1 \end{bmatrix}$	$\begin{bmatrix} \ddots & & 0 \\ & \ddots & \\ 0 & & \ddots \end{bmatrix}$	$d_{i,i} = -2\sin[(i-0.5)\pi/(2N+1)]$ $(i = 1, \ldots, N)$
D-N	$\begin{bmatrix} 1 & & & \\ -1 & \ddots & & \\ & \ddots & -1 & 1 \end{bmatrix}$	$\begin{bmatrix} \ddots & & 0 \\ & \ddots & \\ 0 & & \ddots \end{bmatrix}$	$d_{i,i} = 2\sin[(i-0.5)\pi/(2N+1)]$ $(i = 1, \ldots, N)$
D-D	$\begin{bmatrix} 1 & & & \\ -1 & \ddots & & \\ & \ddots & & \\ & & 1 & \\ & & & -1 \end{bmatrix}$	$\begin{bmatrix} 0 & \longrightarrow & 0 \\ & \ddots & \\ & & \ddots \end{bmatrix}$	$d_{i+1,i} = 2\sin[i\pi/(2N+2)]$ $(i = 1, \ldots, N)$
N-N	$\begin{bmatrix} -1 & 1 & & \\ & \ddots & & \\ & & -1 & 1 \end{bmatrix}$	$\begin{bmatrix} 0 & & \ddots & \\ | & & & \ddots \\ 0 & & & \end{bmatrix}$	$d_{i-1,i} = 2\sin[i\pi/(2N+2)]$ $(i = 2, \ldots, N)$

Table 2.2. First-order difference matrices in the original and the transformed domain for the various boundary conditions.

Therefore, the boundary conditions of the field obtained by taking a difference operation of a original field, $(\partial\phi \,/\, \partial x)$, becomes dual condition of the boundary condition of the original field, ϕ. That is, if the boundary condition of the original field, ϕ, is Neumann-Dirichlet along the x direction, the boundary condition of its derivative with respect to x becomes Dirichlet-Neumann along the x direction.

In the two-dimensional discretization of the three-dimensional problem, as shown in Fig. 2.5, the field of the whole region is considered as a collection of Nx * Nz constituent line fields which is represented by an Nx by Nz matrix as follows.

$$\phi(x,y,z) \dashrightarrow [\phi_{i,j}(y)] = \begin{bmatrix} \phi_{1,1} & \cdot & \cdot & \phi_{1,Nz} \\ \cdot & & & \cdot \\ \cdot & & & \cdot \\ \phi_{Nx,1} & \cdot & \cdot & \phi_{Nx,Nz} \end{bmatrix} \tag{2.6}$$

where the $\phi_{i,j}$ represents the field of the (i,j)-th line.

For the first-order derivative of ϕ with respect to the x-direction, one obtains

$$\frac{\partial\phi(x,y,z)}{\partial x} \dashrightarrow \left.\frac{\partial\phi}{\partial x}\right|_{\substack{x=i\Delta x \\ z=(j-1/2)\Delta z}} = \frac{\phi_{i+1,j}-\phi_{i,j}}{\Delta x}, \quad i = 1, ..., N_x \tag{2.7}$$

or, in matrix notation:

$$\Delta x \frac{\partial \phi}{\partial x} \dashrightarrow \begin{bmatrix} 1 & & & \\ -1 & & & \\ & \ddots & \ddots & \\ & & -1 & 1 \end{bmatrix} \begin{bmatrix} \phi_{1,1} & \cdot & \cdot & \phi_{1,Nz} \\ \cdot & & & \cdot \\ \cdot & & & \cdot \\ \phi_{Nx,1} & \cdot & \cdot & \phi_{Nx,Nz} \end{bmatrix} = [D_x] \, [\phi_{i,j}] \qquad (2.8)$$

The difference matrix $[D_x]$ depends on the lateral boundary condition for ϕ. As shown above, it has the same form of operator matrix as used in the case of one-dimensional discretization. Here, it forms the difference between two successive rows of matrix $[\phi_{i,j}]$.

Analogously, the difference operator for the first-order derivative of ϕ with respect to the z-direction should form the difference between two successive columns of the matrix $[\phi_{i,j}]$. Thus, the difference matrix $[D_z]$, as taken from the Table 2.2 for the N-D boundary condition with the size $N = N_z$, will operate on the transpose of the matrix $[\phi_{i,j}]$.

$$\Delta z \frac{\partial \phi}{\partial z} \dashrightarrow [D_z] [\phi_{i,j}]^t \qquad (2.9)$$

or

$$\dashrightarrow [\phi_{i,j}] [D_z]^t \qquad (2.10)$$

The expression in equation (2.10) is compatible with the difference operators for the x-direction. For example,

$$\Delta x \, \Delta z \frac{\partial^2 \phi}{\partial x \partial z} \dashrightarrow [D_x] [\phi_{i,j}] [D_z]^t \qquad (2.11)$$

2.2.2.2. Second-Order Difference Operator

Using the central difference scheme, the second-order derivative with respect to x is approximated by

$$\frac{\partial^2 \phi(x,y)}{\partial x^2} \quad ---> \quad \frac{\partial^2 \phi}{\partial x^2}\bigg|_{x=x_i} = \frac{\phi_{i+1} - 2\phi_i + \phi_{i-1}}{\Delta x^2} \qquad \text{for } i = 1 \text{ to } N \qquad (2.12)$$

which can be written in a matrix form,

$$\Delta x^2 \frac{\partial^2 \phi(x,y)}{\partial x} \quad ---> \quad
\begin{bmatrix}
1 & -2 & 1 & & & & \\
& 1 & -2 & 1 & & & 0 \\
& & \cdot & \cdot & \cdot & & \\
& & & \cdot & \cdot & \cdot & \\
0 & & & & 1 & -2 & 1
\end{bmatrix}
\begin{bmatrix}
\phi_0 \\
\phi_1 \\
\cdot \\
\cdot \\
\phi_N \\
\phi_{N+1}
\end{bmatrix}
= -[D_{xx}][\phi_i] \qquad (2.13)$$

where $[D_{xx}]$ represents the second-order difference operator wth respect to x. The second-order difference operators shown in Table 2.3 are obtained by imposing the boundary conditions of the field , Table 2.1, to equation (2.13).

The same results for the second-order difference operators can be easily obtained by using the dual boundary condition property of the derivative operation and equations (2.4) and (2.5); that is,

$\Delta x^2 \, \partial^2 \phi \, / \, \partial x^2$

$$\text{--->} \left[D_x^{NN}\right]\left[D_x^{DD}\right]\left[\phi_i\right] = -\left[D_x^{DD}\right]^t\left[D_x^{DD}\right]\left[\phi_i\right] = -\left[D_{xx}^{DD}\right]\left[\phi_i\right] \tag{2.14a}$$

$$\text{--->} \left[D_x^{DD}\right]\left[D_x^{NN}\right]\left[\phi_i\right] = -\left[D_x^{NN}\right]^t\left[D_x^{NN}\right]\left[\phi_i\right] = -\left[D_{xx}^{NN}\right]\left[\phi_i\right] \tag{2.14b}$$

$$\text{--->} \left[D_x^{ND}\right]\left[D_x^{DN}\right]\left[\phi_i\right] = -\left[D_x^{DN}\right]^t\left[D_x^{DN}\right]\left[\phi_i\right] = -\left[D_{xx}^{DN}\right]\left[\phi_i\right] \tag{2.14c}$$

$$\text{--->} \left[D_x^{DN}\right]\left[D_x^{ND}\right]\left[\phi_i\right] = -\left[D_x^{ND}\right]^t\left[D_x^{ND}\right]\left[\phi_i\right] = -\left[D_{xx}^{ND}\right]\left[\phi_i\right] \tag{2.14d}$$

Although the results shown in Table 2.3 are derived from the derivative with respect to x, they can be used for the derivatives with respective to the other variables.

2.2.3. Diagonalization Transformation Matrix

Since the second-order difference operators with respect to x, $[D_{xx}]$, are real symmetric matrices as shown in Table 2.3, they can be transformed into the diagonal matrices by means of orthonormal transformation matries $[T_x]$:

$$[T_x^{DD}]^t \, [D_{xx}^{DD}] \, [T_x^{DD}] = \text{diag} \, [d_{xx}^{DD}] \tag{2.15a}$$

$$[T_x^{NN}]^t \, [D_{xx}^{NN}] \, [T_x^{NN}] = \text{diag} \, [d_{xx}^{NN}] \tag{2.15b}$$

$$[T_x^{DN}]^t \, [D_{xx}^{DN}] \, [T_x^{DN}] = \text{diag} \, [d_{xx}^{DN}] \tag{2.15c}$$

$$[T_x^{ND}]^t \, [D_{xx}^{ND}] \, [T_x^{ND}] = \text{diag} \, [d_{xx}^{ND}] \tag{2.15d}$$

and

$$[T_x^{DD}]^t \, [T_x^{DD}] = [T_x^{NN}]^t \, [T_x^{NN}] = [T_x^{DN}]^t \, [T_x^{DN}] = [T_x^{ND}]^t \, [T_x^{ND}] = I_{Nx} \tag{2.16}$$

boundary conditions left-right	Dxx	Tij
N-D	$$\begin{bmatrix} 1 & -1 & & & & \\ -1 & 2 & -1 & & & \\ & & \ddots & & & \\ & & & -1 & 2 & -1 \\ & & & & -1 & 2 \end{bmatrix}$$	$\sqrt{2/(N+0.5)} \cos[(i-0.5)(j-0.5)\pi/(N+0.5)]$ $(i, j = 1, \ldots, N)$
D-N	$$\begin{bmatrix} 2 & -1 & & & & \\ -1 & 2 & -1 & & & \\ & & \ddots & & & \\ & & & -1 & 2 & -1 \\ & & & & -1 & 1 \end{bmatrix}$$	$\sqrt{2/(N+0.5)} \sin[(i)(j-0.5)\pi/(N+0.5)]$ $(i, j = 1, \ldots, N)$
D-D	$$\begin{bmatrix} 2 & -1 & & & & \\ -1 & 2 & -1 & & & \\ & & \ddots & & & \\ & & & -1 & 2 & -1 \\ & & & & -1 & 2 \end{bmatrix}$$	$\sqrt{2/(N+1)} \sin[(i)(j)\pi/(N+1)]$ $(i, j = 1, \ldots, N)$
N-N	$$\begin{bmatrix} 1 & -1 & & & & \\ -1 & 2 & -1 & & & \\ & & \ddots & & & \\ & & & -1 & 2 & -1 \\ & & & & -1 & 1 \end{bmatrix}$$	$\sqrt{2/N} \cos[(i-0.5)(j-1)\pi/N] \; ; j > 1$ $\sqrt{2/N} \; ; j = 1$ $(i, j = 1, \ldots, N)$

Table 2.3. Second-order difference matrices and elements of the transformation

matrices.

where I_{Nx} represents the Nx by Nx unit matrix, and "diag" means a diagonal matrix.

As indicated in equations (2.15a~d), the transformation matrices are different depending on the boundary condition of the second-order difference operator. The formula for the calculation of the elements of the transformation matrices are summarized in Table 2.3 (see Apendix 1 for the derivation).

Similarly, the first-order difference operators can be (quasi-)diagonalized by using the same transformation matrices (see Appendix 2 for the derivation)

$$\left[T_x^{NN}\right]^t \left[D_x^{DD}\right] \left[T_x^{DD}\right] = \begin{bmatrix} 0 \\ \mathrm{diag}\left[d_x^{DD}\right] \end{bmatrix} \tag{2.17a}$$

$$\left[T_x^{DD}\right]^t \left[D_x^{NN}\right] \left[T_x^{NN}\right] = \begin{bmatrix} 0 & \mathrm{diag}\left[d_x^{NN}\right] \end{bmatrix} \tag{2.17b}$$

$$\left[T_x^{ND}\right]^t \left[D_x^{DN}\right] \left[T_x^{DN}\right] = \mathrm{diag}\left[d_x^{DN}\right] \tag{2.17c}$$

$$\left[T_x^{DN}\right]^t \left[D_x^{ND}\right] \left[T_x^{ND}\right] = \mathrm{diag}\left[d_x^{ND}\right] \tag{2.17d}$$

Comparison of equations (2.17a~d) with equations (2.15a~d) shows that the diagonalization of the first-order difference matrix requires the pre-multiplication of the transpose of the transformation matrix for the dual boundary condition. The forms of the diagonalized matrices and the formula for the calculation of the diagonal elements are shown in Table 2.2.

The diagonal elements of the diagonalized second-order difference matrices can be calculated using equations(2.14a~d) and (2.16). That is,

$$\mathrm{diag}\left[d_{xx}^{DD}\right] = \left[T_x^{DD}\right]^t \left[D_{xx}^{DD}\right] \left[T_x^{DD}\right]$$

$$= - [T_x^{DD}]^t [D_x^{LD}]^t [T_x^{NN}][T_x^{NN}]^t [D_x^{DD}] [T_x^{DD}]$$

$$= - [d_x^{DD}]^t [d_x^{DD}] \qquad\qquad (2.18a)$$

$$\text{diag } [d_{xx}^{NN}] = [T_x^{NN}]^t [D_{xx}^{NN}] [T_x^{NN}]$$

$$= - [T_x^{NN}]^t [D_x^{NN}]^t [T_x^{DD}][T_x^{DD}]^t [D_x^{NN}] [T_x^{NN}]$$

$$= - [d_x^{NN}]^t [d_x^{NN}] \qquad\qquad (2.18b)$$

$$\text{diag } [d_{xx}^{DN}] = [T_x^{DN}]^t [D_{xx}^{DN}] [T_x^{DN}]$$

$$= - [T_x^{DN}]^t [D_x^{DN}]^t [T_x^{ND}][T_x^{ND}]^t [D_x^{DN}] [T_x^{DN}]$$

$$= - [d_x^{DN}]^t [d_x^{DN}] \qquad\qquad (2.18c)$$

$$\text{diag } [d_{xx}^{ND}] = [T_x^{ND}]^t [D_{xx}^{ND}] [T_x^{ND}]$$

$$= - [T_x^{ND}]^t [D_x^{ND}]^t [T_x^{DN}][T_x^{DN}]^t [D_x^{ND}] [T_x^{ND}]$$

$$= - [d_x^{ND}]^t [d_x^{ND}] \qquad\qquad (2.18d)$$

2.3. Summary

In this chapter, the outline of the proposed method was described briefly and the discrete matheties related to the method of lines was explained. The proposed method makes use of the structural feature of a planar circuit: that is, the spaces above and below the substrate surface are uniform and homogeneous. As a result, the space is discretized only in the two-dimensional substrate surface and an analytical solution is used for the normal direction.

The descretization scheme used in the method of lines depends on the boundary condition of the field of interest. This shifted descretization scheme reduces the discretization error and makes the formulation symmetric. Also, the discrete

forms of the first-order derivative and the second-order derivative were derived, in which the side wall boundary conditions were incorporated. Finally, the diagonalization of the first-order difference matrix and the second-order difference matrix were explained by orthogonal transformation matrices.

Chapter 3

Time-Domain Method of Lines Applied to a Partially Filled Waveguide

3.1. Introduction

Since this is the first time the Time-Domain Method of Lines has been used in the solution of the time-dependent Maxwell's equations, a simple problem will be used as a test case to check the validity of the method. The simplest possilble structure to analyze is the homogeneously filled rectangular waveguide excited by an electric field, E_z, infinite in length and uniform in the z (axial) direction so that a simple two-dimensional problem results. However, the formulation to be described in this chapter is for the partially filled rectangular waveguide structure shown in Fig. 3.1. This is appropriate because the solution to the homogeneously filled rectangular
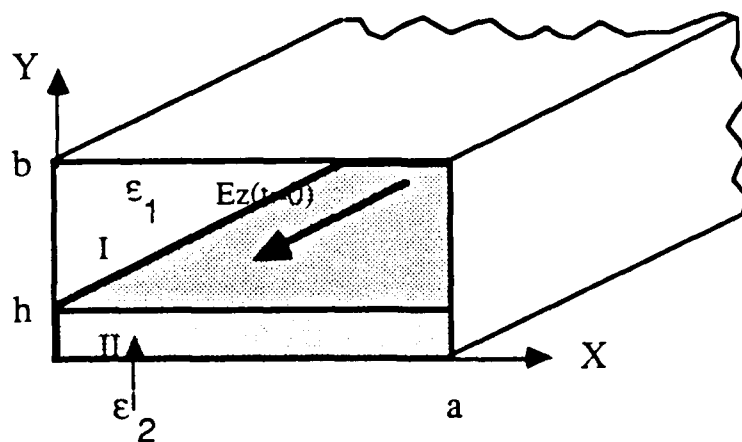

Fig. 3.1 Structure of a partially filled rectangular waveguide.

waveguide can be obtained as a special case of the partially filled waveguide by using the same dielectric constant for region I and region II.

3.2. Formulation

As shown in Fig. 3.1, the problem is to find a behavior of an input pulse in a partially filled rectangular waveguide excited by an electric field, E_z, infinite in length and uniform in the z (axial) direction. The structure can be reduced to a two-dimensional one because of the input condition. The formulation for such a problem is simple, yet it contains all the essential features of the proposed method. This problem corresponds to finding the cutoff frequencies of various TM to z modes in the frequency domain [31]. Such information can be extracted from the time-domain data obtained by the method described below.

The starting point of formulation is the time-dependent Maxwell's equations expressed in scalar notation; that is,

$$\partial E_z / \partial y - \partial E_y / \partial z = -\mu \, \partial H_x / \partial t \qquad (3.1a)$$

$$\partial E_x / \partial z - \partial E_z / \partial x = -\mu \, \partial H_y / \partial t \qquad (3.1b)$$

$$\partial E_y / \partial x - \partial E_x / \partial y = -\mu \, \partial H_z / \partial t \qquad (3.1c)$$

$$\partial H_z / \partial y - \partial H_y / \partial z = \epsilon(y) \, \partial E_x / \partial t \qquad (3.1d)$$

$$\partial H_x / \partial z - \partial H_z / \partial x = \epsilon(y) \, \partial E_y / \partial t \qquad (3.1e)$$

$$\partial H_y / \partial x - \partial H_x / \partial y = \epsilon(y) \, \partial E_z / \partial t \qquad (3.1f)$$

Because of the excitation, only E_z, H_x and H_y exist and $\partial / \partial z = 0$. Then, equations (3.1a~f) are reduced to

$$-\mu\, \partial H_x / \partial t = \partial E_z / \partial y \qquad\qquad (3.2a)$$

$$-\mu\, \partial H_y / \partial t = - \partial E_z / \partial x \qquad\qquad (3.2b)$$

$$\varepsilon(y)\, \partial E_z / \partial t = \partial H_y / \partial x - \partial H_x / \partial y \qquad\qquad (3.2c)$$

The time-dependent wave equation for the E_z field derived from Maxwell's equations (3.2a~c) is

$$\partial^2 E_z / \partial x^2 + \partial^2 E_z / \partial^2 y - \mu\varepsilon(y)\, \partial^2 E_z / \partial^2 t = 0 \qquad\qquad (3.3)$$

Notice that the side wall boundary condition for E_z and H_x is Dirichlet-Dirichlet and that of Hy is Neumann-Neumann. Figure 3.2 shows the cross-sectional
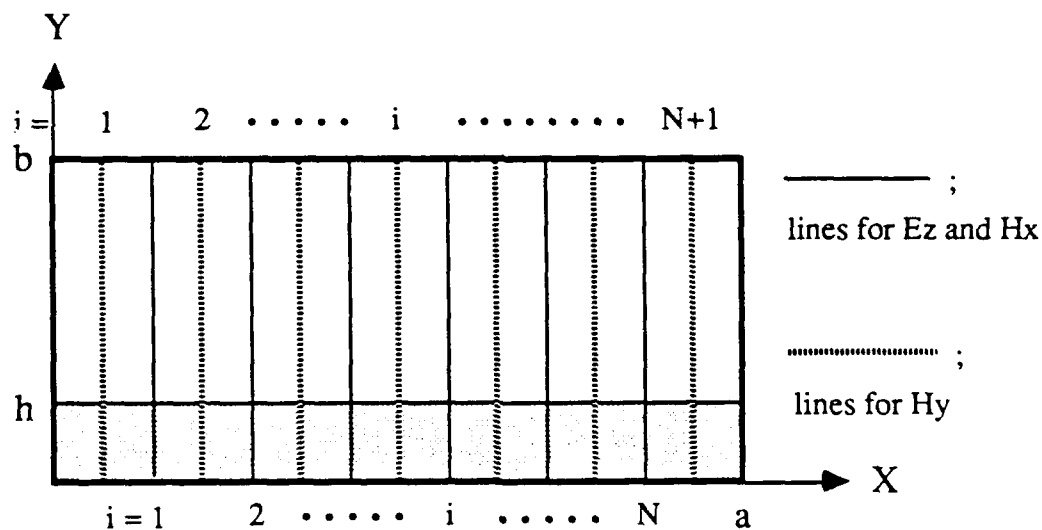

Fig. 3.2. Discretization lines for Ez, Hx, and Hy incorporating the boundary conditions.

view of the structure shown in Fig. 3.1 with the appropriate discretized field lines determined by the rule described in Section 2.2.1. Now the time-domain Maxwell's equations and the wave equation are discretized in the x-direction only.

$$-\mu\, \partial[H_x] / \partial t = \partial[E_z] / \partial y \tag{3.4a}$$

$$-\mu\, \partial[H_y] / \partial t = - [D_x^{DD}] [F_z] / \Delta x \tag{3.4b}$$

$$\varepsilon(y)\, \partial[E_z] / \partial t = [D_x^{NN}] [H_y] / \Delta x - \partial[H_x] / \partial y \tag{3.4c}$$

$$[D_{xx}^{DD}][E_z] / (\Delta x)^2 + \partial^2[E_z] / \partial y^2 - \mu\varepsilon(y)\, \partial^2[E_z] / \partial t^2 = 0 \tag{3.5}$$

where $[D_x^{DD}]$, $[D_x^{NN}]$ are the first-order difference operators and $[D_{xx}^{DD}]$ is the second-order difference operator, in which the side wall boundary condition is incorporated as explained in Section 2.2.2. The variables $[E_z]$, $[H_x]$ and $[H_y]$ are column vectors with elements which are actually functions of y and t. The i-th element of the column vector represents the field along i-th line in Fig. 3.2.

If the solution for $[E_z]$ is found using equation (3.5), the other field components are obtained from the equations (3.4a~c). However, it is very difficult to solve the wave equation (3.5) directly because the equation represents a set of coupled partial differential equations due to $[D_{xx}^{DD}]$. Since $[D_{xx}^{DD}]$ is a real symmetric matrix, there exists a real orthonormal matrix $[T_x^{DD}]$ that transforms $[D_{xx}^{DD}]$ into a diagonal matrix $[d_{xx}^{DD}]$ as explained in Section 2.2.3.

Using equations (2.15a) and (2.17a and b), the coupled partial differential equations, (3.4a~c) and (3.5), can now be transformed into a diagonalized form as follows.

$$- \mu \frac{\partial \left[\widetilde{H_x} \right]}{\partial t} = \frac{\partial \left[\widetilde{E_z} \right]}{\partial y}$$

(3.6a)

$$- \mu \frac{\partial \left[\widetilde{H_y} \right]}{\partial t} = \frac{1}{\Delta x} \left[d_x^{DD} \right] \left[\widetilde{E_z} \right]$$

(3.6b)

$$- \varepsilon(y) \frac{\partial \left[\widetilde{E_z} \right]}{\partial t} = \frac{1}{\Delta x} \left[d_x^{NN} \right] \left[\widetilde{H_y} \right] - \frac{\partial \left[\widetilde{H_x} \right]}{\partial y}$$

(3.6c)

$$\frac{1}{\Delta x^2} \left[d_{xx}^{DD} \right] \left[\widetilde{E_z} \right] + \frac{\partial^2 \left[\widetilde{E_z} \right]}{\partial y^2} - \mu \varepsilon(y) \frac{\partial^2 \left[\widetilde{E_z} \right]}{\partial t^2} = [0]$$

(3.7)

where ~ represents the transformed field corresponding to the real field without ~. The transformation of the real field is accompanied by the diagonalization of the first-order and the second-order difference matrices.

$$\left[\widetilde{E_z} \right] \equiv \left[T_x^{DD} \right]^t \left[E_z \right]$$

(3.8a)

$$\left[\widetilde{H_x} \right] \equiv \left[T_x^{DD} \right]^t \left[H_x \right]$$

(3.8b)

$$\left[\widetilde{H_y} \right] \equiv \left[T_x^{NN} \right]^t \left[H_y \right] = - \left[T_x^{DD} \right] \left[H_y \right]$$

(3.8c)

Notice that equation (3.7) represents a set of uncoupled partial differential equations. That is, it can be solved independently along the i-th line. A typical equation describing the transformed field along the i-th line is

$$\frac{\partial^2}{\partial y^2} \widetilde{E_{z,i}} + \frac{d_{xx,i}^{DD}}{\Delta x^2} \widetilde{E_{z,i}} - \mu \varepsilon(y) \frac{\partial^2}{\partial t^2} \widetilde{E_{z,i}} = 0$$

(3.9)

with the boundary conditions,

$$\widetilde{E_{z,i}}(y=0) = \widetilde{E_{z,i}}(y=b) = 0 \tag{3.10a}$$

$$\widetilde{E_{z,i}}(y=h^-) = \widetilde{E_{z,i}}(y=h^+) \tag{3.10b}$$

Using the separation of variables technique, one can obtain the solution for the i-th line

$$\widetilde{E_{zi}}(y,t) =$$

$$\lceil \ \Sigma_n \ (A_{ni} \cos \omega_{ni}t + B_{ni} \sin \omega_{ni}t) \ \underline{\sin K1_{ni}(b-y)} \ , \qquad \text{for region I}$$

$$\lfloor \ \Sigma_n \ (A_{ni} \cos \omega_{ni}t + B_{ni} \sin \omega_{ni}t) \ \underline{(\sin K1_{ni}d \ / \sin K2_{ni}h) \sin K2_{ni}y} \ ,$$

$$\text{for region II} \quad (3.11)$$

where $K1_{ni}$, $K2_{ni}$ and ω_{ni} are determined by the characteristic transcendental equations derived from the interface boundary condition (3.10b).

$$K1_{ni} \cos K1_{ni}d \sin K2_{ni}h + K2_{ni} \sin K1_{ni}d \cos K2_{ni}h = 0 \tag{3.12a}$$

$$\omega_{ni}^2 = [(K1_{ni})^2 - d_{xxi}^{DD} / (\Delta x)^2] / \mu\varepsilon_1$$

$$= [(K2_{ni})^2 - d_{xxi}^{DD} / (\Delta x)^2] / \mu\varepsilon_2 \tag{3.12b}$$

Notice that for a given n in equation (3.11), the underlined part constitutes the n-th mode on the i-th line, $\widetilde{E_{zni}}(y)$.

$$\widetilde{E_{zni}}(y) =$$

$$\lceil \ \sin K1_{ni}(b-y), \qquad\qquad\qquad\qquad \text{in region I}$$

$$\lfloor \ (\sin K1_{ni}d \ / \sin K2_{ni}h) \sin K2_{ni}y \ , \qquad\qquad \text{in region II} \quad (3.13)$$

From this point on, there are basically two approaches. First, by knowing the initial conditions for E_z, one can find A_{ni} using the orthogonal property of the modes [32].

$$A_{ni} = \frac{\int_0^b \widetilde{E_{zi}}(t=0)\, \mu_0 \varepsilon(y)\, \widetilde{E_{zni}}(y)\, dy}{\int_0^b \widetilde{E_{zni}}(y)^2 \mu_0 \varepsilon(y)\, dy} \qquad (3.14)$$

One way to determine B_{ni} is to use the causality condition for H_x and H_y, which states

$$\widetilde{H_{x,i}}(y, t = -\frac{\Delta t}{2}) = \widetilde{H_{y,i}}(y, t = -\frac{\Delta t}{2}) = 0 \qquad (3.15)$$

where Δt is the unit time interval in the sampling process. The expressions for H_{xi} and H_{yi} can be found by integrating equations (3.6a and b) with respect to t.

$$\widetilde{H_{x,i}}(t) = -\frac{1}{\mu_0} \int \frac{\partial \widetilde{E_{z,i}}}{\partial y}\, dt$$

$$= \frac{1}{\mu_0} \Sigma_n \left\{ K_{ni} \left(-B_{ni} \frac{\cos \omega_{ni} t}{\omega_{ni}} + A_{ni} \frac{\sin \omega_{ni} t}{\omega_{ni}} \right) \cos K_{ni} y \right\} \qquad (3.16a)$$

$$\widetilde{H_{y,i}}(t) = -\frac{d_x^{DD}}{\mu_0 \Delta x} \int \widetilde{E_{z,i}}\, dt$$

$$= \frac{d_{x,i}^{DD}}{\mu_0 \Delta x} \Sigma_n \left\{ K_{ni} \left(- B_{ni} \frac{\cos \omega_{ni} t}{\omega_{ni}} + A_{ni} \frac{\sin \omega_{ni} t}{\omega_{ni}} \right) \sin K_{ni} y \right\} \quad \text{(3.16b)}$$

Imposing the causality condition. equation (3.15), to equations (3.16a and b), one can obtain

$$B_{ni} = -A_{ni} \tan (\omega_{ni} \Delta t / 2) \quad \text{(3.17)}$$

After A_{ni} and B_{ni} are determined, the solution at any point and time can be found by using equation (3.11). Then, the real field can be obtained by the inverse transform.

$$[E_z(y,t)] = \left[T_x^{DD} \right] \left[\widetilde{E}_z(y,t) \right] \quad \text{(3.18)}$$

Second, an alternative method is the application of a time-stepping procedure, where equations (3.6a~c) are discretized in time:

$$\widetilde{H_{x,i}}(y,N + \tfrac{1}{2}) = \widetilde{H_{x,i}}(y,N - \tfrac{1}{2}) - \frac{\Delta t}{\mu_0} \frac{\partial}{\partial y} \widetilde{E_{z,i}}(y,N) \quad \text{(3.19a)}$$

$$\widetilde{H_{y,i}}(y,N + \tfrac{1}{2}) = \widetilde{H_{y,i}}(y,N - \tfrac{1}{2}) + \frac{\Delta t}{\mu_0} \frac{d_{xi}^{DD}}{\Delta x} \widetilde{E_{z,i}}(y,N) \quad \text{(3.19b)}$$

$$\widetilde{E_{z,i}}(y,N+1) = \widetilde{E_{z,i}}(y,N) - \frac{\Delta t}{\varepsilon(y)} \frac{d_{xi}^{DD}}{\Delta x} \widetilde{H_{y,i}}(y,N + \tfrac{1}{2}) - \frac{\Delta t}{\varepsilon(y)} \frac{\partial}{\partial y} \widetilde{H_{x,i}}(y,N + \tfrac{1}{2}) \quad \text{(3.19c)}$$

From the initial condition of E_z, one can find A_{ni} at time $t = 0$ using equation (3.14). We denote this quantity as $A_{ni}{}^N$ with $N = 0$. The solution (3.11) at the sime step N can now be expressed in the form

$$\widetilde{E_{zi}^N}(y) =$$

$\lceil \Sigma_n A_{ni}{}^N \sin K1_{ni}(b-y),$ in region I

$\lfloor \Sigma_n A_{ni}{}^N (\sin K1_{ni}d / \sin K2_{ni}h) \sin K2_{ni}y,$ in region II   (3.20a)

Similarly, for H_{xi} and H_{yi} at the time step $(N + 1/2)$,

$$\widetilde{H_{xi}^{N+1/2}}(y) =$$

$\lceil \Sigma_n B_{ni}{}^{N+1/2} \cos K1_{ni}(b-y),$ in region I

$\lfloor \Sigma_n B_{ni}{}^{N+1/2} (\cos K1_{ni}d / \cos K2_{ni}h) \cos K2_{ni}y,$ in region II   (3.20b)

$$\widetilde{H_{yi}^{N+1/2}}(y) =$$

$\lceil \Sigma_n C_{ni}{}^{N+1/2} \sin K1_{ni}(b-y),$ in region I

$\lfloor \Sigma_n C_{ni}{}^{N+1/2} (\sin K1_{ni}d / \sin K2_{ni}h) \sin K2_{ni}y,$ in region II   (3.20c)

Substituting the equations for the fields, (3.20a~c), into equations (3.19a~c), a leap-frog type iteration scheme [1?] can be implemented to calculate the coefficients of modal fields on the i-th line at any time step N.

$$B_{ni}^{N+1/2} = B_{ni}^{N-1/2} + \frac{\Delta t}{\mu_0} K_{ni} A_{ni}^N$$

$$(3.21a)$$

$$C_{ni}^{N+1/2} = C_{ni}^{N-1/2} + \frac{1}{\mu_0} \frac{\Delta t}{\Delta x} d_{x,i}^{DD} A_{ni}^{N}$$

(3.21b)

$$A_{ni}^{N+1} = A_{ni}^{N} - \frac{1}{\epsilon(y)} \frac{\Delta t}{\Delta x} d_{x,i}^{NN} C_{ni}^{N+1/2} - \frac{\Delta t}{\epsilon(y)} K_{n,i} B_{ni}^{N+1/2}$$

(3.21c)

where K_{ni} becomes either $K1_{ni}$ or $K2_{ni}$ depending on the region. After the coefficients at the N-th time step are determined, the transformed field can be obtained by the equations (3.20a~3). The real field at the N-th time step can be obtained by invoking the inverse transformation as described above to $\left[\widetilde{E}_z \right]^N$.

After the history of pulse scattering is obtained in the time-domain, the cutoff frequency spectrum of the structure can be extracted via the Fourier transform of the time-domain data. If the time-domain data consists of N data points with unit sampling time Δt, the resolution of the frequency domain information is $\Delta f = 1 / N\Delta t$, and the maximum frequency range that can be obtained is $N\Delta f/2$.

For comparison, the cutoff spectrum of the same structure can also be calculated analytically by using the transverse resonance technique. For TM to z mode (LSE mode), the eigenvalue equation is given by [32]

$$p \tan (qh) = -q \tan (pd)$$

(3.22a)

$$p^2 = \epsilon_1 \omega^2 \mu_0 \epsilon_0 - (n\pi/a)^2$$

(3.22b)

$$q^2 = \epsilon_2 \omega^2 \mu_0 \epsilon_0 - (n\pi/a)^2, \quad \text{for } n = 1, ...$$

(3.22c)

3.3. Results and Discussion

3.3.1. Homogeneously Filled Rectangular Waveguide

The structure considered has dimensions: a = 2 [cm], b = 1 [cm], $\varepsilon_1 = 3$, and $\varepsilon_2 = 3$. Figure 3.3 depicts the E_z field distributions in the waveguide cross-section (x-y plane) at each time step after a pulsed E_z excitation is imposed at $\bar{t} = 0$ at the center of the cross section. Figure 3.4 shows the spectrum of the time signal of E_z where the waveguide cutoff frequencies are represented by the peaks. The cutoff frequencies obtained by present method differ by less than one percent from the analytical values.

3.3.2. Partially Filled Rectangular Waveguide

The structure is ; a = 2 [cm], b = 1 [cm], h = 0.3 [cm], $\varepsilon_1 = 1$, and $\varepsilon_2 = 3$. Figure 3.5 depicts the E_z field distributions in the waveguide cross section (x-y plane) after a pulsed E_z excitation is imposed at t = 0 at the center of the cross section. Figure 3.6 shows the spectrum of the time signal of E_z where the waveguide cutoff frequencies are represented by the peaks. The cutoff frequencies obtained differ by less than one percent from the analytical values.

It should be noted that the two approaches (the modal expansion and the time-stepping) described above should be equivalent in principle. However, each has advantages and disadvantages. For instance, if one deals with a time-dependent excitation, the time-stepping method would be simpler to implement. Otherwise, the modal expansion method is more efficient as long as only the results at a particular time are of interest. However, if any frequency-domain information is needed, the time history needs to be found. The first method needs to be used at many time instances. The time-stepping method automatically generates the time history. Hence, the amount of computation would be about the same. In many cases, there
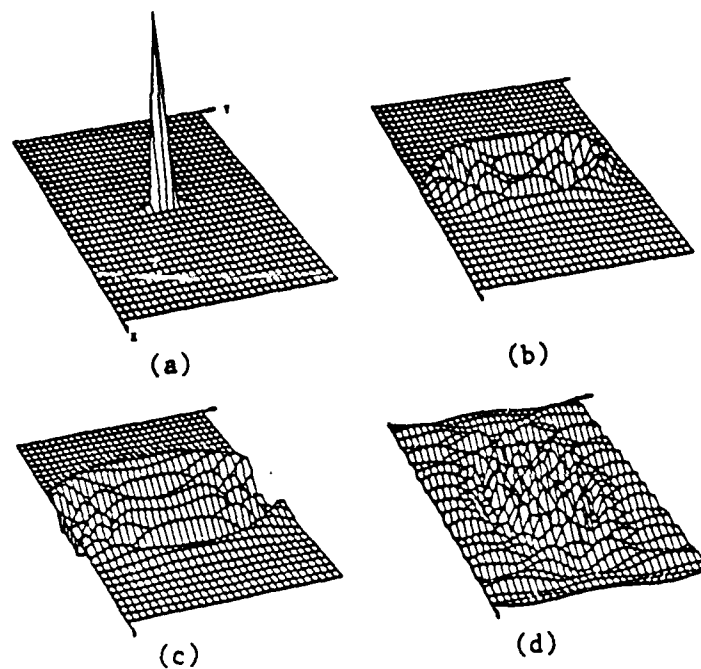
Fig. 3.3 The Ez-pulse scattering in a homogeneously filled rectangular waveguide

(a=2, b=1 cm, ε =3). (a) t=0, (b) t=20, (c) t=30 and (d) t=80 p-sec.
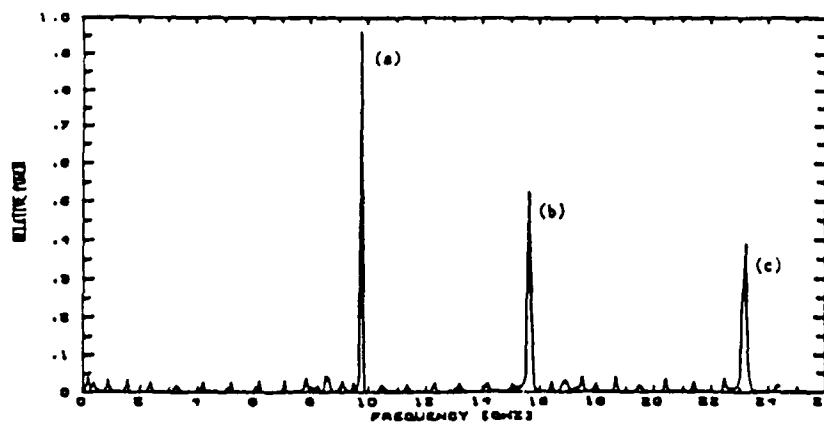
Fig. 3.4 The cutoff frequency spectrum of the homogeneously filled waveguide

when the initial input is placed at the center of the waveguide.

(a) TM11, (b) TM31 and (c) TM51 modes
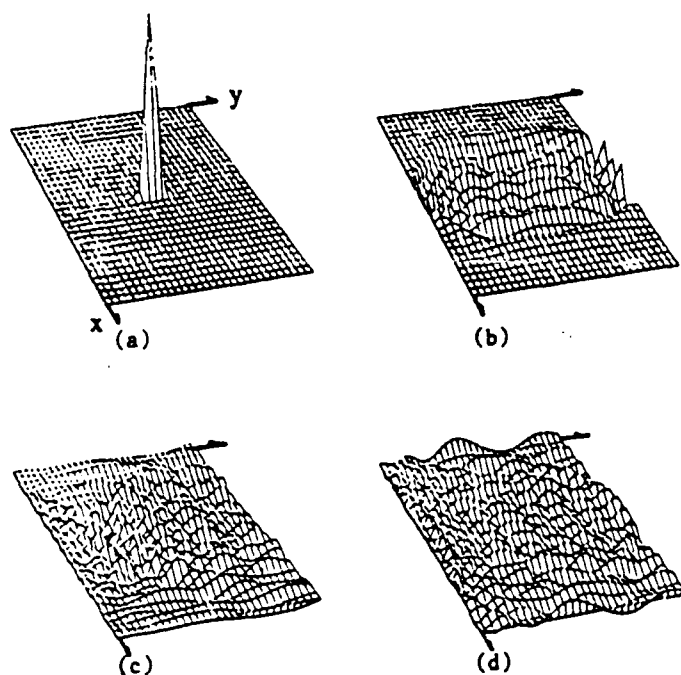
Fig. 3.5 The Ez-pulse scattering in a partially filled rectangular waveguide

(a=2, b=1, h=.3 [cm], $\varepsilon 1=1$, and $\varepsilon 2=3$).

(a) t=0, (b) t=20, (c) t=40 and (d) t=60 p-sec.
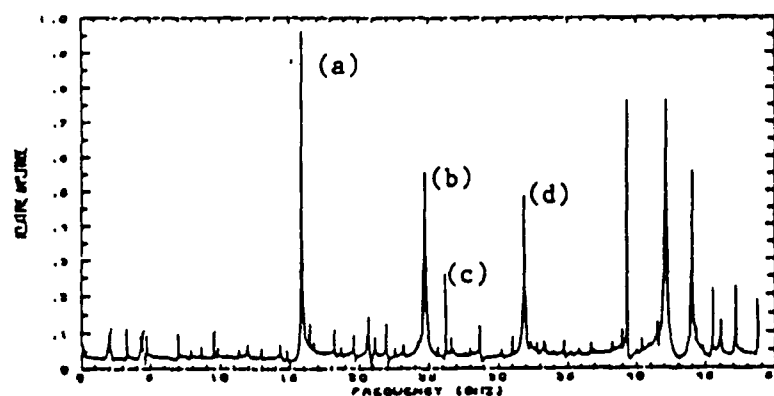
Fig. 3.6 The cutoff frequency spectrum of the partially filled waveguide when

the initial input is placed at the center of the waveguide.

(a) TM11, (b) TM31, (c) TM12 and (d) TM32 modes

are ambiguities in finding the initial condition for the time derivative. In such instances, it may be simpler to use time stepping to generate the time history required. Finally, it is also possible to switch from one method to the other.

3.4. Conclusions

A new time-domain technique is presented in which an analytical process is incoporated along one of the spatial dimensions so that the dimensions of the problem are effectively reduced by one. The present approach can be used to calculate the cutoff frequency of other planar transmission structures and can be extended to propagation problems. It has a number of potential advantages over many other time domain methods. First, the method is believed to be efficient since much analytical processing is used. Second, the problem can handle open boundaries in the vertical (y) direction because of the analytical solutions used in y.

Chapter 4
Time-Domain Method of Lines Applied to Finned Waveguide

4.1. Introduction

A new time-domain method was studied for a partially filled rectangular waveguide in the Chapter 3 in which the interface boundary condition is not changed along one of the spatial dimensions (transformed direction). Therefore, the problem could be reduced into a one-dimensional boundary value problem which requires only one-dimensional discretization.

In the previous chapter, the feasibility of a new time-domain method was shown by calculating the cutoff frequencies of the partially filled waveguide problem accurately. In this chapter, the method will be extended to a structure which contains a metallic strip at the interface boundary. This extension also makes use of the Method of Lines and an analytical process can be incorporated along one of the spatial dimensions. However, because of the non-uniform boundary condition in the transformed direction, each line is not independent but related to each other in order to match the required interface boundary conditions. Consequently, instead of considering one-dimensional eigenmodes for each line as in the case of the uniform interface boundary condition problem, two-dimensional eigenmodes should be considered in this structure [33].

40

4.2. Formulation

As shown in Fig. 4.1, the problem is to find the time-domain behavior of an input pulse in a uniform rectangular waveguide excited by an electric field infinite in length and uniform in the z-direction. The structure can be reduced to a two-dimensional one because of the input condition. This problem corresponds to finding the time-domain behavior of the pulsed input and the cutoff spectrum of the given structure. The formulation is very similar to the partially filled waveguide problem except for the treatment of the interface boundary condition.
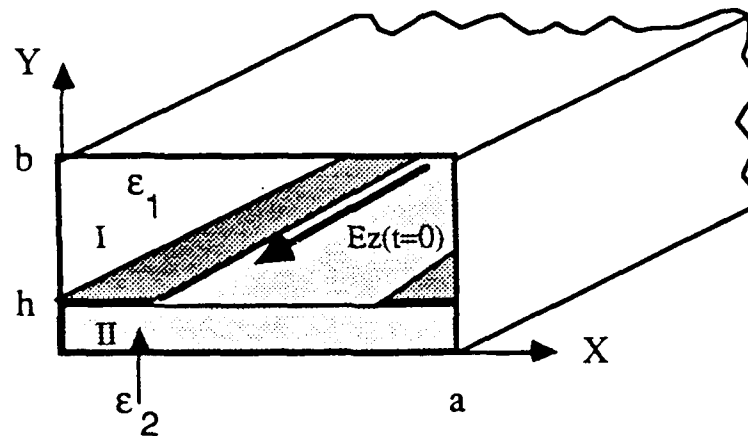

Fig. 4.1 Structure of a finned rectangular waveguide.

Because of the excitation, only E_z, H_x and H_y exist and $\partial / \partial z = 0$. Also, notice that the side wall boundary condition of the fields E_z, H_x is Dirichlet-Dirichlet and that of H_y is Neumann-Neumann. Since the structure is uniform in the space above and below the $y = h$ axis, the time-domain equations are discretized in the x-direction only. Figure 4.2 shows the cross-sectional view of the finned rectangular

waveguide with the appropriate discretized field lines incoporating the boundary conditions. Now, Maxwell's equations in (3.1a~f) are reduced and discretized to
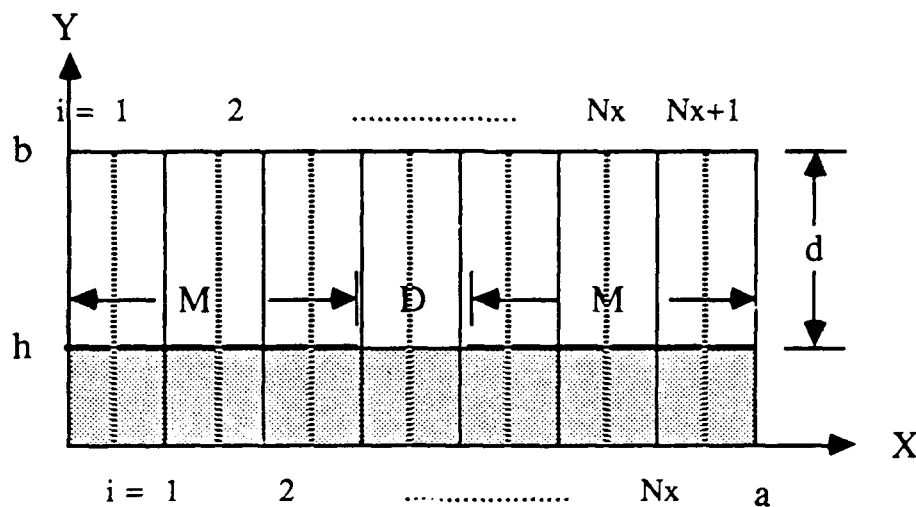

Fig. 4.2. The cross-sectional structure of a finned rectangular waveguide.

$$-\mu\, \partial[H_x] / \partial t = \partial[E_z] / \partial y \qquad (4.1a)$$

$$-\mu\, \partial[H_y] / \partial t = [D_x^{DD}]\, [E_z] / \Delta x \qquad (4.1b)$$

$$\varepsilon(y)\, \partial[E_z] / \partial t = [D_x^{NN}]\, [H_y] / \Delta x - \partial[H_x] / \partial y \qquad (4.1c)$$

The governing equation for E_z is

$$[D_{xx}^{DD}][E_z] / (\Delta x)^2 + \partial^2[E_z] / \partial y^2 - \mu\varepsilon(y)\, \partial^2[E_z] / \partial t^2 = 0 \qquad (4.2)$$

with appropriate boundary conditions ;

$$[E_z(t,y=h+)] = [E_z(t,y=h-)], \text{ for all } t \text{ and } i \qquad (4.3a)$$

$[H_x(t,y=h-)] - [H_x(t,y=h+)] = [J_z(t,y=h)]$, for all t and i   (4.3b)

$[E_z(t,y=h)] = 0$, for all t and i on M   (4.3c)

$[E_z(t,y=0)] = [E_z(t,y=b)] = 0$, for all t and i   (4.3d)

where $[D_x^{DD}]$, $[D_x^{NN}]$, $[D_{xx}^{DD}]$ are difference operators in which the side wall boundary condition is incorporated (see Tables 2.2 and 2.3). The variables $[E_z]$, $[H_x]$ and $[H_y]$ are column vectors representing the fields along each line and are functions of y and t. Notice that equation (4.2) is a system of a coupled partial differential equations.

Since $[D_{xx}^{DD}]$ is a real symmetric matrix, there exists a real orthogonal matrix $[T_x^{DD}]$ that transforms $[D_{xx}^{DD}]$ into a diagonal matrix $[d_{xx}^{DD}]$. We can now transform the real field $[E_z]$ into a transformed field $[\tilde{E}_z] = [T_x^{DD}]^t [E_z]$ where the superscript t stands for transpose. The transform of equation (4.2) is

$$\frac{1}{\Delta x^2}\left[d_{xx}^{DD}\right]\left[\tilde{E}_z\right] + \frac{\partial^2}{\partial y^2}\left[\tilde{E}_z\right] - \mu\varepsilon(y)\frac{\partial^2}{\partial t^2}\left[\tilde{E}_z\right] = [0]$$

(4.4)

with the transformed boundary conditions of (4.3a~d)

$$\left[\tilde{E}_z(t, y=h^+)\right] = \left[\tilde{E}_z(t, y=h^-)\right], \text{ for all t and i}$$ (4.5a)

$$\left[\tilde{H}_x(t, y=h^+)\right] - \left[\tilde{H}_x(t, y=h^-)\right] = -\left[\tilde{J}_z(t, y=h)\right], \text{ for all t and i}$$ (4.5b)

$$\left[\tilde{E}_z(t, y=h)\right] = \text{unknown}, \text{ for all t and i on M}$$ (4.5c)

$$\left[\tilde{E}_z(t, y=0)\right] = \left[\tilde{E}_z(t, y=b)\right] = [0], \text{ for all t and i}$$ (4.5d)

Notice that equation (4.4) is a set of uncoupled partial differential equations related by non-uniform boundary conditions (4.3a~c). For the i-th line, equations (4.4) ~ (4.5c) become

$$\frac{d_{xx,i}^{DD}}{\Delta x^2} \widetilde{E_{z,i}} + \frac{\partial^2}{\partial y^2} \widetilde{E_{z,i}} - \mu\varepsilon(y) \frac{\partial^2}{\partial t^2} \widetilde{E_{z,i}} = 0$$

(4.6)

$$\widetilde{E_{z,i}}(t, y=h^+) = \widetilde{E_{z,i}}(t, y=h^-)$$

(4.7a)

$$\widetilde{H_{x,i}}(t, y=h^+) - \widetilde{H_{x,i}}(t, y=h^-) = -\widetilde{J_{z,i}}(t, y=h)$$

(4.7b)

$$\widetilde{E_{z,i}}(t, y=h) = unknown$$

(4.7c)

$$\widetilde{E_{z,i}}(t, y=0) = \widetilde{E_{z,i}}(t, y=b) = 0$$

(4.7d)

By means of the separation of variables technique, the intermediate solution on the i-th line for the n-th mode which satisfies the transformed boundary condition, (4.5a and d), is

$$\widetilde{E_{zni}}(t,y) =$$

$(A_{ni} \cos \omega_{ni}t + B_{ni} \sin \omega_{ni}t) \sin K1_{ni}(b-y)$, in region I

$(A_{ni} \cos \omega_{ni}t + B_{ni} \sin \omega_{ni}t)(\sin K1_{ni}d / \sin K2_{ni}h) \sin K2_{ni}y$, in region II

(4.8a)

where $K1_{ni}$, $K2_{ni}$, and ω_{ni} are related by

$$K1_{ni}^2 = \omega_{ni}^2 \mu\varepsilon_1 + d_{xxi}^{DD} / (\Delta x)^2$$

$$K2_{ni}^2 = \omega_{ni}^2 \mu\varepsilon_2 + d_{xxi}^{DD} / (\Delta x)^2$$

(4.8b)

The modal current $[J_{zn}]$ obtained from the discontinuity of the corresponding modal magnetic field $[H_{xn}]$ at $y = h$ by using (4.1a) is

$$\widetilde{J_{x,ni}}(t, y=h) = -\frac{f_{ni}(t)}{\mu} \frac{\sin K1_n d}{\sin K2_n h} K2_{ni} \cos K2_n h + K1_{ni} \cos K1_n d$$

$$= \widetilde{Y_{ni}}(t, y=h) \, \widetilde{E_{z,ni}}(t, y=h) \tag{4.9a}$$

where $f_{ni}(t) = (A_{ni} \sin \omega_{ni} t / \omega_{ni} - B_{ni} \cos \omega_{ni} t / \omega_{ni})$ (4.9b)

$$\widetilde{Y_{ni}} = -\frac{1}{\mu} \frac{1}{\omega_{ni}} \frac{A_{ni} \sin \omega_{ni} t - B_{ni} \cos \omega_{ni} t}{A_{ni} \cos \omega_{ni} t - B_{ni} \sin \omega_{ni} t} (K1_{ni} \cot K1_n d + K2_{ni} \cot K2_n h)$$

(4.9c)

Now, the final boundary condition, (4.3b), is applied in the real field domain.

$$[J_{z,n}] = \left[T_x^{DD}\right] \left[\widetilde{Y_n}\right] \left[T_x^{DD}\right]^t [E_{z,n}] \tag{4.10}$$

where $[Y_n(t, y=h)]$ is the diagonal admitance matrix with diagonal elements given by equation (4.9c). Because $J_{zni} = 0$ if i is on the non-metallic portion (D) and $E_{zni} = 0$ if i is on the metallic portion (M), the characteristic matrix equation can be derived.from equation (4.10).

$$[J_{z,ni}]_{i\,on\,D} = \left\{ \left[T_x^{DD}\right] \left[\widetilde{Y_n}\right] \left[T_x^{DD}\right]^t \right\}_{red} [E_{z,ni}]_{i\,on\,D} \tag{4.11}$$

where "D" represents the non-metalization portion of the substrate surface as shown in Fig. 4.2 and the subscript "red" represents the reduced matrix obtained from the

full matrix in { } by removing the rows and columns corresponding to the metalization portion.

In order for the n-th eigenmode, $[E_{zn}]$, to satisfy (4.11) at all times with a non-trivial solution, the time-dependent solution for each line should have the same functional form except for a constant factor, and the determinant of the reduced matrix should be zero. The final solution of the $[E_{zn}]$ is

$$\widetilde{E_{zni}}(t,y) =$$

$$\left\lceil (A_n \cos \omega_n t + B_n \sin \omega_n t)\, C_{ni} \sin K1_{ni}(b-y), \quad \text{in region I} \right.$$

$$\left\lfloor (A_n \cos \omega_n t + B_n \sin \omega_n t)\, C_{ni} (\sin K1_{ni}d / \sin K2_{ni}h) \sin K2_{ni}y, \quad \text{in region II} \right.$$

$$(4.12)$$

where ω_n is n-th eigenvalue of the characteristic equation given by

$$\det \left\{ \left[T_x^{DD} \right] \left[\widetilde{Y_n} \right] \left[T_x^{DD} \right]^t \right\}_{red} = 0 \qquad (4.13)$$

and the coefficients, C_{ni}, can be derived from the eigenvector, $[E_{zn}]$, of (4.11) corresponding to the n-th eigenvalue. The procedure described above is very similar to the frequency-domain method of lines [28].

Finally, any real field can be expanded in terms of the eigenmodes in the transformed domain

$$\widetilde{E_{zi}}(t,y) =$$

$$\left\lceil \sum_n (A_n \cos \omega_n t + B_n \sin \omega_n t)\, C_{ni} \underline{\sin K1_{ni}(b-y)}, \quad \text{in region I} \right.$$

$$\left\lfloor \sum_n (A_n \cos \omega_n t + B_n \sin \omega_n t)\, C_{ni} \underline{(\sin K1_{ni}d / \sin K2_{ni}h) \sin K2_{ni}y}, \right.$$

$$\text{in region II} \qquad (4.14)$$

Notice that for a given n in equation (4.14), the underlined part constitutes the n-th mode of the i-th line

$$\widetilde{E_{z,ni}}(y) =$$

$$\lceil \frac{\sin K1_{ni}(b-y)}{}, \quad \text{in region I} \tag{4.15a}$$

$$\lfloor \frac{\sin K1_{ni}d}{\sin K2_{ni}h} \sin K2_{ni}y , \quad \text{in region II} \tag{4.15b}$$

In equation (4.14), A_n can be found from the initial condition of $\left[\widehat{E}_z(t=0,y)\right] = \left[T_x^{DD}\right]^t \left[E_z(t=0,y)\right]$ and orthogonality property

$$A_n = \frac{\displaystyle\int_0^b \left[\widetilde{E}_z(t=0,y)\right]^t \left[\widetilde{E_{zn}}(y)\right] dy}{\displaystyle\int_0^b \left[\widetilde{E_{zn}}(y)\right]^t \left[\widetilde{E_{zn}}(y)\right] dy} \tag{4.16}$$

Also, the causality condition assumed by time iteration method [34] can be used to find B_n

$$B_n = A_n \tan(\omega_n \Delta t / 2), \quad \text{where } \Delta t \leq \Delta x / \sqrt{2} C_{max} \tag{4.17}$$

where C_{max} is the maximum wave phase velocity within the structure. The real field at any time can be obtained by invoking the inverse transformation to the transformed field, $\left[\widetilde{E}_z(t,y=y_0)\right]$;

$$[E_z] = \left[T_x^{DD}\right]\left[\widetilde{E}_z\right] \tag{4.18}$$

4.3. Results and Discussion

The structure of the finned waveguide considered is a = 1 [cm], b = 2 [cm], h = 0.5 [cm], M = 0.25 [cm], ε_1 = 3, and ε_2 = 3. To check the validity of the method, the eigenfrequency of the finned rectangular waveguide for the dominant TE mode was found and compared with Hoefer's result [24] in Fig. 4.3. Good agreement was
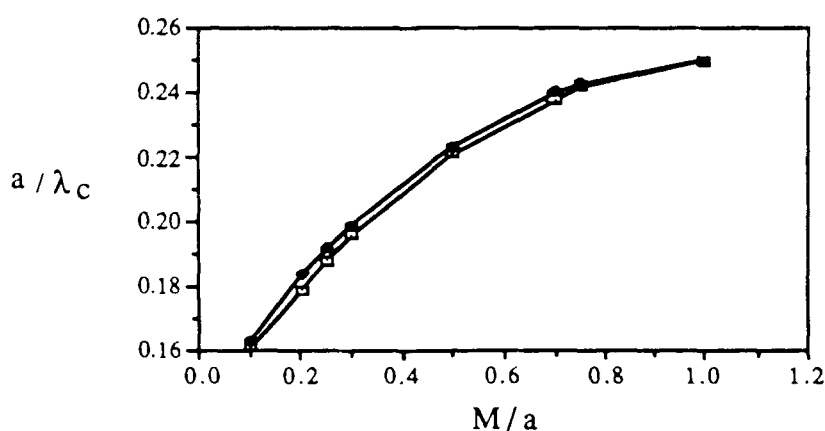

Fig. 4.3. Cutoff frequency of the fined waveguide shown in Fig 4.2

with b/a=2, h=1.

(light squares ; present method, dark squares ; Hoefer [24])

obtained. For further confirmation, the E_z field distributions in the homogeneously filled rectangular waveguide are calculated by the present two-dimensional method, and the result is compared with that obtained by the one-dimensional method described in the Chapter 3. Figure 4.4 shows the result. Even though the ripple seems to be higher than that of the one-dimensional analysis, the result shows that the wave scattering characteristics can be analyzed by the two-dimensional time-domain

method. The pulse propagation and scattering in the finned rectangular waveguide is dipicted in Fig. 4.5.
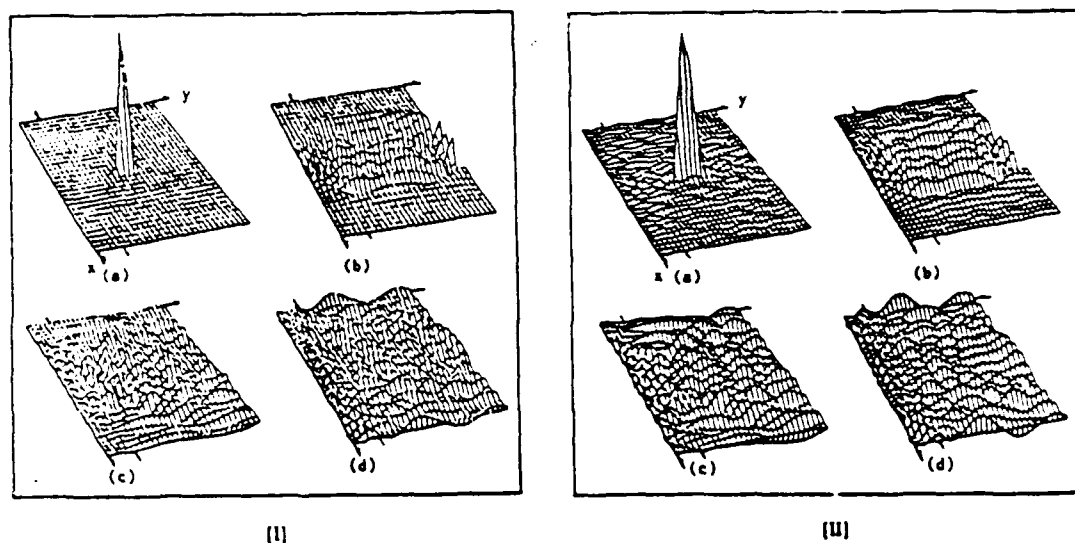

Fig. 4.4. Pictures of a pulse scattering in a partially filled rectangular waveguide

with a=2, b=1, h=.3, $\varepsilon 1=1$, $\varepsilon 2=3$. ([I] ; one-dimensional method,

[II] ; two-dimensional method)

(a) t=0, (b) t=20, (c) t=40, and (d) t=60 [p-sec]

4.4. Conclusions

In this chapter, it was shown that the two-dimensional Time-Domain Method of Lines can be used to analyze planar transmission structures which have a non-uniform boundary condition at the interface boundary along the transformed direction. This is accomplished by the two-dimensional eigenmode expansion concept instead of the one-dimensional method used in the case of the uniform boundary problem.
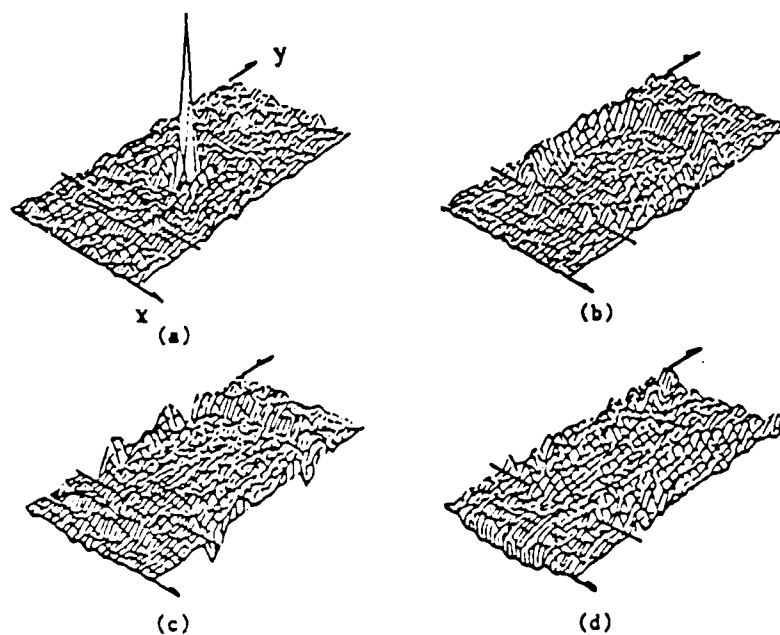
Fig. 4.5. Pictures of a Ez pulse scattering in a finned rectangular waveguide

with a=1, b=2, h=0.5, M=0.25, and $\varepsilon 1= \varepsilon 2=3$.

(a) t=0, (b) t=30, (c) T=40, and (d) t=60 [p-sec]

Chapter 5

Characterization of Uniform Microstrip Line and its Discontinuities using Time-Domain Method of Lines

5.1. Introduction

In the previous chapters, the TDML has been applied to the two-dimensional problems to obtain the scattering data of the input pulse in the time domain. The cutoff frequency spectrums of planar transmission lines were extracted from the time-domain data via the Fourier transform. Although the cutoff frequency is an important parameter characterizing a waveguide structure, the propagation characteristics are even more important to the microwave circuit designer. In this chapter, it will be shown that the TDML can be extended to the three-dimensional propagation problems. The time-domain behavior of the input pulse in a planar transmission line circuit can be obtained by TDML. From the time-domain data, the frequency domain characteristics for a wide range of frequencies can be found via the Fourier transform. The procedure and the formulation for the characterization of the three-dimensional structure is presented [35]. The characteristics of a uniform microstrip line and its discontinuities (step-in-width, open-end and gap discontinuities) are presented and compared with available published data.
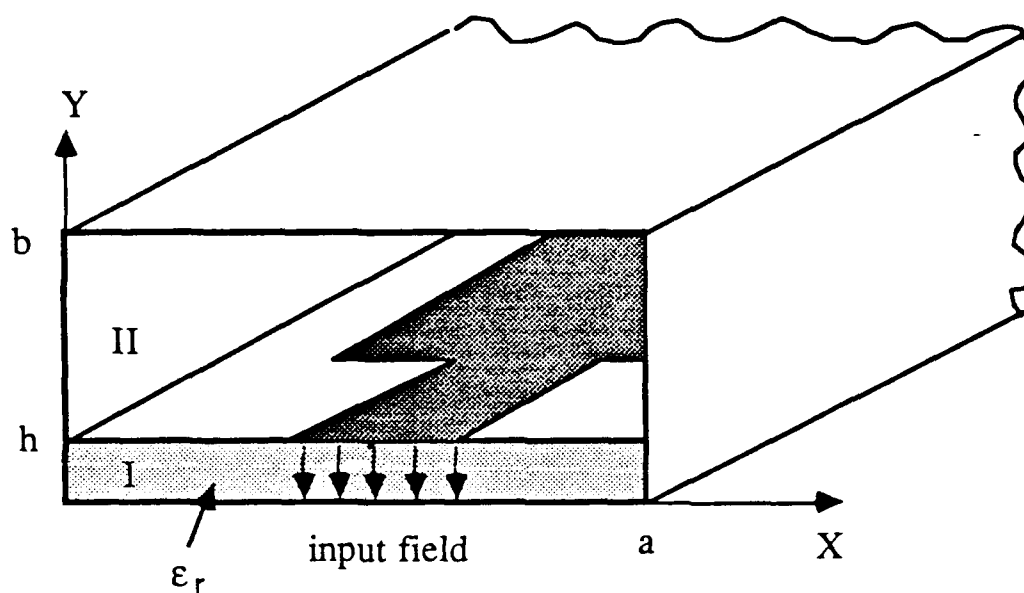
Fig. 5.1 A general planar transmission line with discontinuity in

a shielded rectangular waveguide

5.2. Formulation

Let us consider a general planar transmission line with a discontinuity, as shown in Fig. 5.1. In order to apply the TDML, electric or magnetic walls need to be placed at both ends of the waveguide so that a resonant structure will result. Figure 5.2 shows the top view of the structure with discretization points for the y component of the electric field, E_y. It is assumed that the structure has spatial symmetry in x-direction so that the problem domain can be reduced by a factor of two.

5.2.1. Discretization

As shown in Fig. 5.2, the structure is discretized by field lines which are properly placed to satisfy the boundary conditions on the side walls and the end
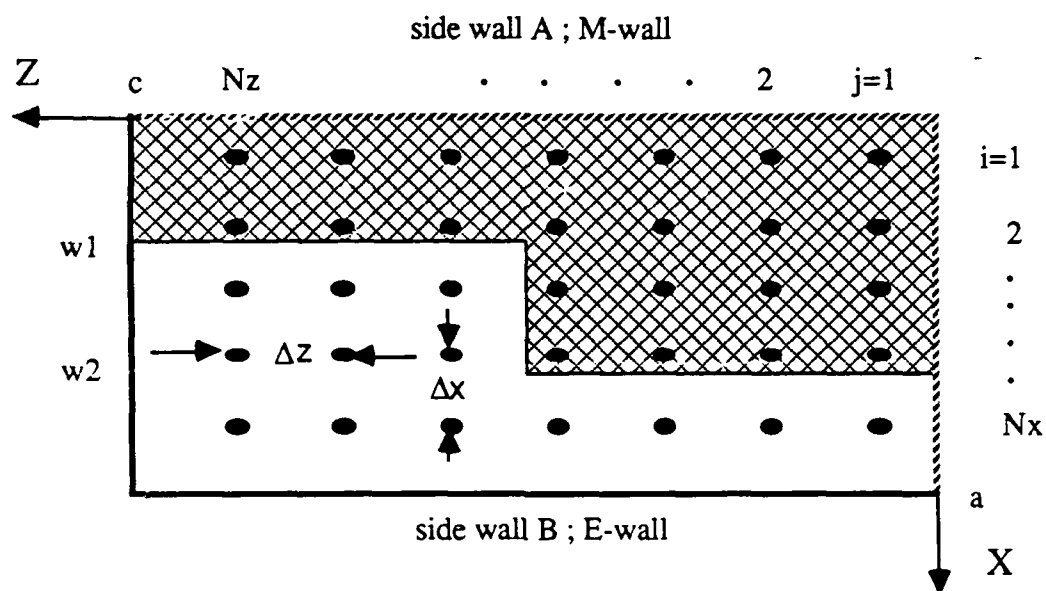
Fig. 5.2 Top view of the structure shown in Fig.5.1 with the proper

discretization points for Ey component

walls. For example, since the Neumann boundary condition for E_y is applied on the side wall A and the Dirichlet condition on the side wall B, the E_y points are located away from the side wall A by one half of Δx and away from side wall B by one Δx. Also, it is important to choose the E_y nodes as the outermost nodes on the strip in order to reduce the error in the calculation of the field distribution. After discretization of the space, the original field in the continuous space is approximated by many field lines parallel to the y-axis at the discretization points

$$E_y(x,y,z,t) \dashrightarrow [E_{y,k}(y,t)]^t = [E_{y,1}, E_{y,2}, ..., E_{y,NxNz}]^t \qquad (5.1)$$

where $k = i + (j-1) N_x, \qquad 1 \le i \le N_x, 1 \le j \le N_z$. $\qquad (5.2)$

5.2.2. Expansion of the Input Pulse

In the structure shown in Fig. 5.1 with end walls, a field distribution at any time t, $[E_y(y,t)]$, can be expanded by modal field distributions, $[E_{yn}(y)]$ as follows;

$$[E_y(y,t)] = \Sigma_n \ (A_n \cos \omega_n t + B_n \sin \omega_n t) \ [E_{yn}(y)] \qquad (5.3)$$

where [ ] denotes a column vector whose i-th component represents the field value at the i-th discretization line as shown in equation (5.1). Also the subscript n denotes the mode number. One thing to be mentioned here is that if the structure and the initial input support any static charge distribution, the DC-mode ($\omega_n = 0$) should be included in equation (5.3) to obtain the correct time- and frequency-domain data.

In the expansion of (5.3), the coefficients A_n can be determined by the input field distribution, $[E_y(y, t=0)]$ and the orthogonal property of the modal fields

$$A_n = \frac{\int_0^b [E_y(y,t=0)]^\dagger [E_{y,n}(y)]\,dy}{\int_0^b [E_{y,n}(y)]^\dagger [E_{y,n}(y)]\,dy} \qquad (5.4)$$

Also, the B_n can be found by the causality condition used in the time iteration method[19, 34]

$$B_n = A_n \tan (\omega_n \Delta t / 2) \qquad (5.5)$$

where $\Delta t \leq \min(\Delta x, \Delta z) / C_{max} \sqrt{3}$ $\qquad (5.6)$

and C_{max} is the maximum wave phase velocity within the structure.

In order to find the engenfrequencies and eigenmodes of the structure, a technique used in frequency-domain Method of Lines [29] is borrowed. In this technique, the characteristic equation is obtained by applying the metallic boundary condition to the metalization on the dielectric interface boundary. The equation is given by (see Apendix 3 for details)

$$\begin{bmatrix} [E_z] \\ [E_x] \end{bmatrix}_{red} = \begin{bmatrix} [G_z] \\ [G_x] \end{bmatrix}_{red} [\rho]_{red} = [0] \quad , \quad \text{for static fields} \tag{5.7a}$$

$$\begin{bmatrix} [E_z] \\ [E_x] \end{bmatrix}_{red} = \begin{bmatrix} [G_{zz}][G_{zx}] \\ [G_{xz}][G_{xx}] \end{bmatrix}_{red} \begin{bmatrix} [J_z] \\ [J_x] \end{bmatrix}_{red} = [0] \quad , \quad \text{for time-harmonic fields} \tag{5.7b}$$

In order to obtain a non-trivial solution of equations (5.7a and b),

$$\det [G(\omega)]_{red} = 0, \quad \text{for time-harmonic fields} \tag{5.8}$$

where the subscript "red" represents the reduced matrix corresponding to the discretization points on the metalization.

After the eigenfrequencies are found, equations (5.7a) and (5.7b) can be used to obtain the charge distribution, $[\rho]^t$, and the current density distributions, $[[J_z],[J_x]]^t$. The modal field distributions, $[E_{yn}(y)]$, can be derived from these quantities. It is found that the system of equations (5.7a) and (5.7b) need to be solved by the QR method [40] to ensure stability of the results.

5.2.3. Time-Domain Data and Frequency-Domain Characteristics

Once the procedures described in Sections 5.2.1 and 5.2.2 are carried out, all the constants in equation (5.3) are determined so that the field value at any point and

time can be calculated. Therefore, the characteristics of a circuit can be obtained by observing the propagation and scattering of the input pulse in the given circuit. In this chapter, four structures will be tested, namely, the uniform microstrip line and three commonly encountered discontinuities (step-in-width, open-end and gap).
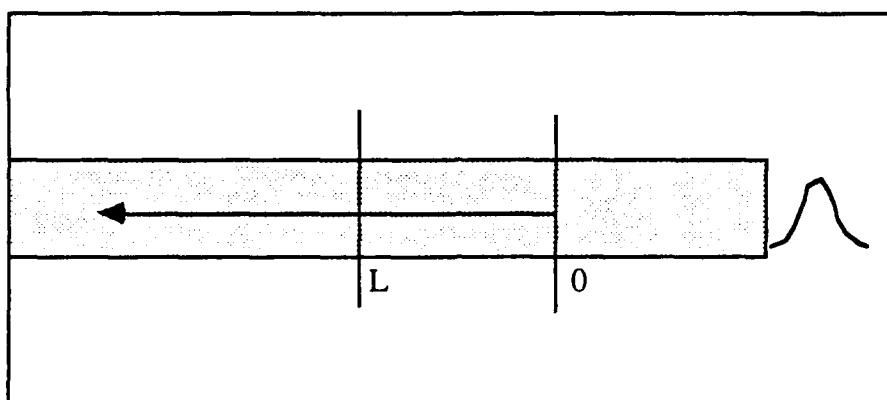

Fig. 5.3 Top view of a uniform microstrip line with two observation planes
and initial input puise.

5.2.3.1. Uniform Microstrip line

Figure 5.3 shows a uniform microstrip line with two observation planes. In this case, the transfer function can be found from

$$\exp[-\gamma(\omega)L] = V_y(\omega, z=L) / V_y(\omega, z=0) \tag{5.9}$$

where $\gamma(\omega) = \alpha(\omega)+j\beta(\omega)$ = propagation constant of the uniform microstrip line.

$V_y(\omega,z=0)$ = Fourier transform of $[V_y(t,z=0)]$ at a fixed x.

$V_y(\omega,z=L)$ = Fourier transform of $[V_y(t,z=L)]$ at a fixed x.

$V_y(t,z)$ is a voltage defined as the line integral of E_y from the microstrip to the ground plane.

$$V_y(t) = \int_h^0 E_y(t,y) \, dy, \quad \text{at fixed x and z}$$

(5.10)

where the integral was evaluated by using the 4-th order Gaussian quadrature. Stable results can be obtained by using this choice of voltage definition for the calculation of the frequency-domain characteristics.

The effective dielectric constant can be derived from the calculated phase constant, β, by

$$\varepsilon_{eff}(\omega) = \beta^2(\omega) / \omega^2 \mu_0 \varepsilon_0$$

(5.11)

The voltage-current definition is used for the characteristic impedance calculation.

$$Z(\omega) = V_y(\omega, z=0) / I_z(\omega, z=0)$$

(5.12)

where the current is found by a line integral of the H-field around the microstrip line at z=0.

$$\int_0^{x_1} H_x(y=y_b) \, dx + \int_{y_a}^{y_t} H_y(x=x_1) \, dy + \int_{x_1}^0 H_x(y=y_t) \, dx$$

(5.13)

5.2.3.2. Discontinities

Figure 5.4 shows a general two-port discontinuity with a uniform microstrip line connected to each port, where two reference planes and two observation planes are indicated. In order to obtain the frequency-dependent scattering parameters of the
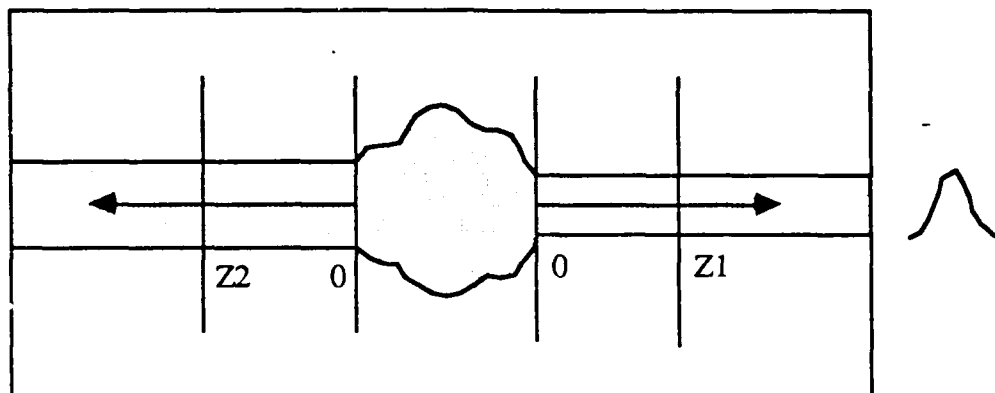
Fig. 5.4 General two-port discontinuity with a uniform microstrip line connected
to each port, where two reference planes and two observation planes are
indicated.

discontinuity, the incident wave, $E_{y,inc}$, and the reflected wave, $E_{y,ref}$, should be calculated at some point on the input observation plane and the transmitted wave, $E_{y,trs}$, at the corresponding point on the output observation plane. Then,

$$S_{11}(\omega) = [V_{y,ref}(\omega,z_1) / V_{y,inc}(\omega,z_1)] / \exp[-2\gamma_1(\omega)z_1] \tag{5.14}$$

$$S_{21}(\omega) = [V_{y,trs}(\omega,z_2) \sqrt{Z_{01}(\omega)} / V_{y,inc}(\omega,z_2) \sqrt{Z_{02}(\omega)}] / \exp[-\gamma_1(\omega)z_1 - \gamma_2(\omega)z_2)] \tag{5.15}$$

where $\gamma_1(\omega)$, $\gamma_2(\omega)$ are the propagation constants of the uniform microstrip lines connected to each port of the discontinuity. Note that only S_{11} exists for a one-port structure, such as an open-end.

5.3. Results and Discussion

In this chapter, four structures on alumina subtrate ($\varepsilon_r \approx 9.6$, h = 0.635 or 0.7 mm) shielded by a rectangular waveguide (a = 2, b = 10, and c = 45 mm) were studied. These are a uniform microstrip line, a step-in-width, an open-end and a gap. In the calculation of the field variation in the time domain, the following number of discretization points were used.

number of discretized points in x-direction $\approx$ 20 (Δx = 0.095 mm)

number of discretized points in z-direction = 100 (Δz = 0.445 mm)

number of modes = 19

As a rule of thumb, the number of discretized points is chosen so that the discretization length is approximately one-tenth the length of the smallest wavelength to be considered.
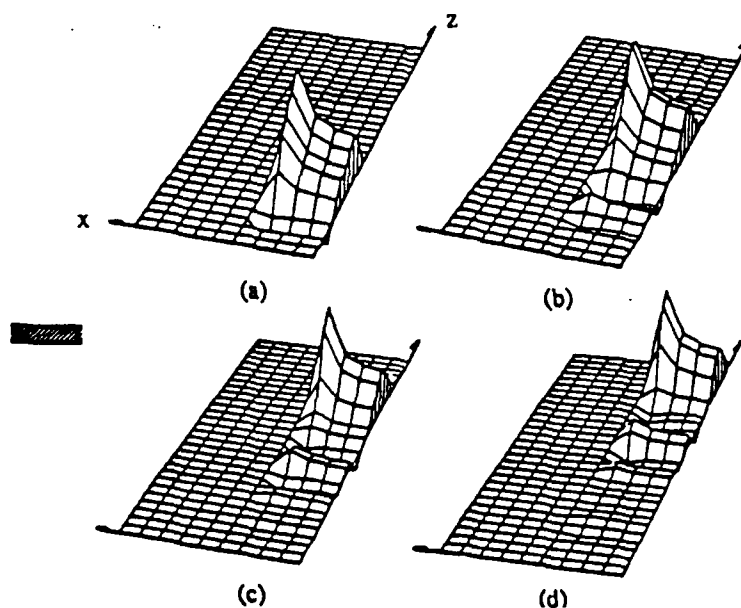

Fig. 5.5 Ey configulation beneath a uniform microstrip line (a=2, b=10, h=0.635, W=0.635 mm) (a) t=0, (b) t=40, (c) t=80 and (d) t=120 p-sec.

Figure 5.5 shows the pulse propagation along the uniform microstrip (h = 0.635, W=0.635 mm) in the time domain. In order to check the convergence of the method with respect to the number of modes, the effective dielectric constant is calculated using a different number of modes. As shown in Fig. 5.6, convergent results can be found by using more than seventeen modes for the tested structure.
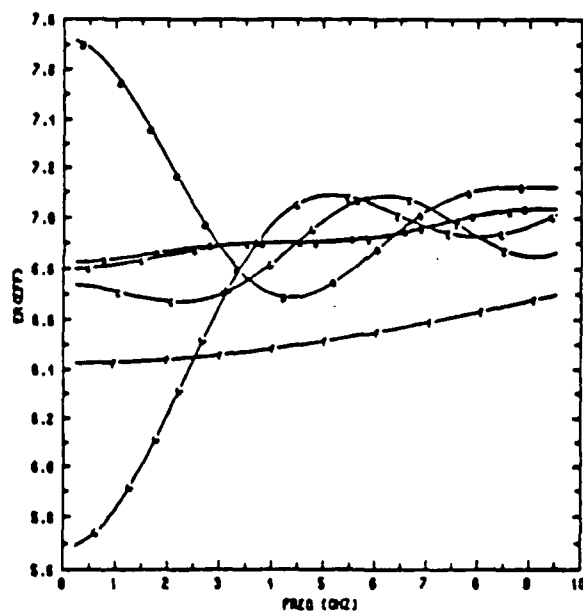

Fig. 5.6 Convergence of the method with respect to the number of modes.

A=19, B=17, C=15, D=13, E=11 and F=curve fit formula [36]

Figure 5.7 shows the propagation constant, β, obtained by using the Fourier transform of the time-domain data shown in Fig. 5.5. The results agree well with those from the curve-fit formula [36]. Figure 5.8 shows the calculated transmission

coefficient which is supposed to be one. The deviation from the exact value is less than 1 %.
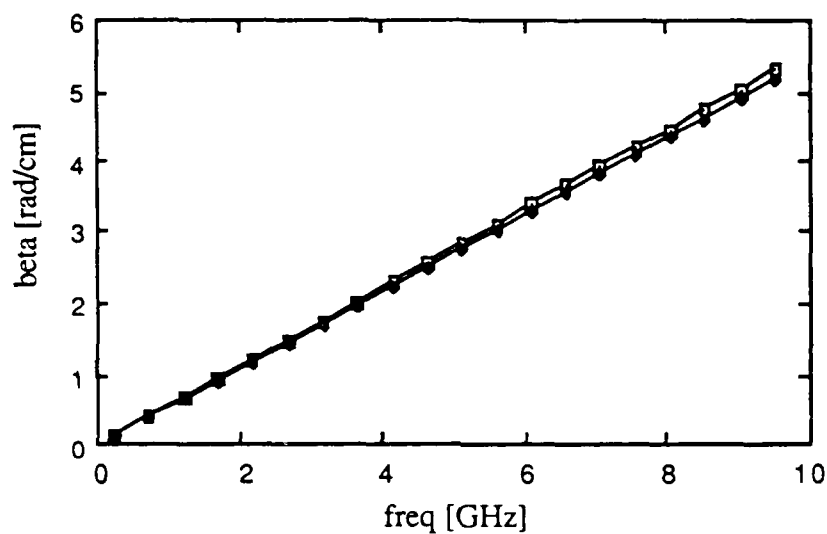
Fig. 5.7 Dispersion relation for the uniform microstrip line (a=2, b=10, h=.635 [mm], $\varepsilon 1$=1, and $\varepsilon 2$=9.6) obtained by TDML.

———□——— TDML , ———●——— curve-fit formula [36] (open structure)

Figure 5.9 shows the characteristic impedance (Z_0) of the structure from both the TDML calculation and the closed form formula given in reference [36]. The difference between the two results is about 6 % and it is believed to be caused by the side wall effect which is known to reduce the characteristic impedance [37].
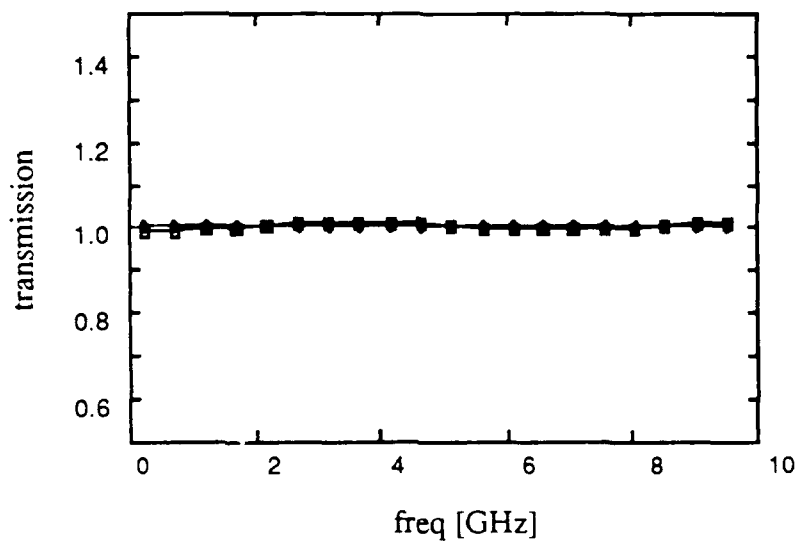
Fig. 5.8 The transmission coefficient (T) of the uniform microstrip line obtained

by TDML.

TDML , exact
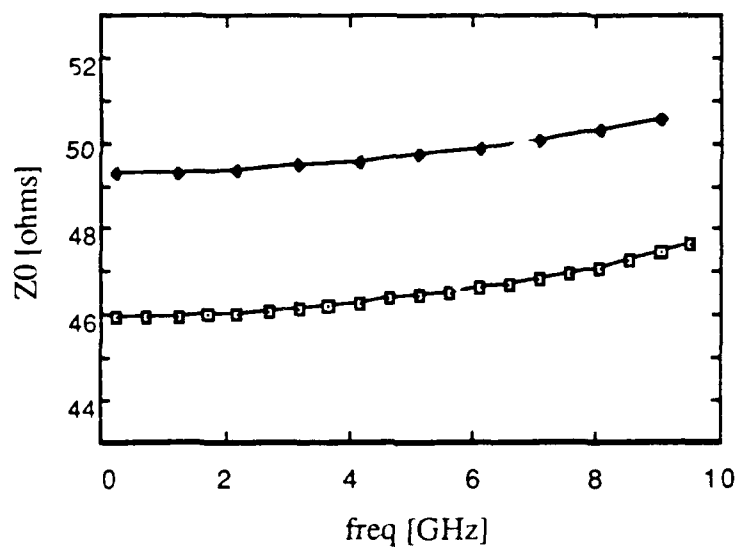
Fig. 5.9 Characteristic impedance for the uniform microstrip line shown in Fig. 5.5.

TDML , curve-fit formula [36] (open structure)
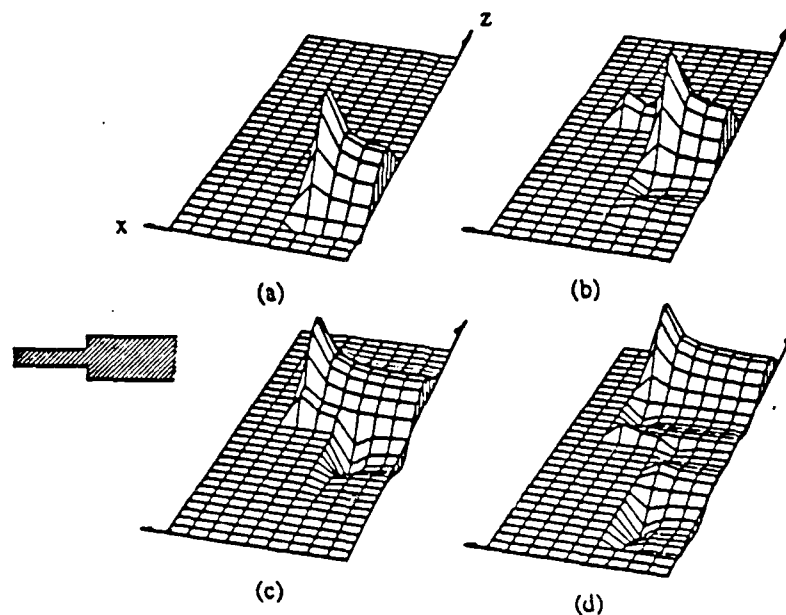
Fig. 5.10 Ey configuration beneath a step discontinuity (a=2, b=10, h=0.635, W1=

1.27, W2=0.635 mm) (a) t=0, (b) t=40, (c) t=80 and (d) t=120 p-sec.
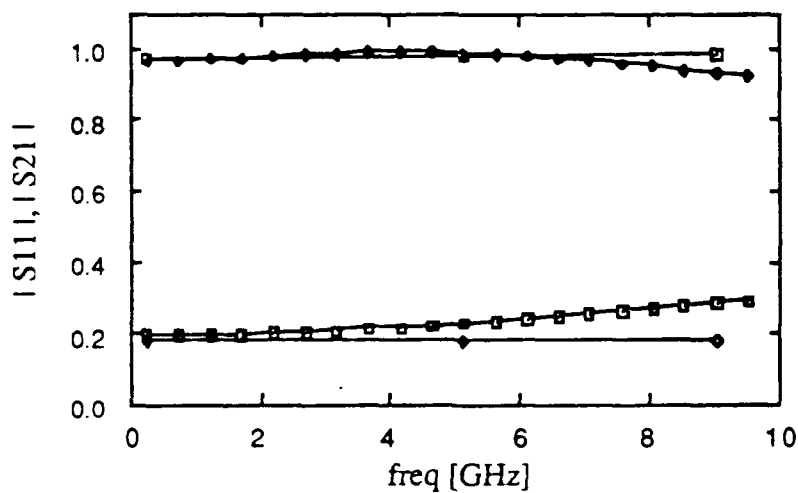
Fig. 5.11 Scattering parameters(S11, S12) for the symmetric step discontinuity

shown in Fig. 5.10.
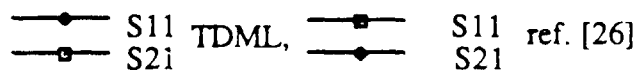
Figure 5.10 shows the scattering of the pulse at a microstrip step discontinuity in the time domain. Using equations (5.14) and (5.15), the frequency-domain characteristics can be extracted from the time-domain data. Figure 5.11 shows the frequency-dependent scattering parameters of the given structure with published data [26].

Figures 5.12 and 5.13 show the scattering of a pulse at a microstrip (h=0.7, W=0.7 mm) open-end and a gap (s=0.35 mm) in the time domain, respectively. The frequency-dependent scattering parameters derived from the time-domain data are shown in Figs. 5.14 and 5.15. Also plotted in these figures for comparison are the FDTD results reported in [26]. The results agree reasonablely well with [26], although they do show some undulation due to discretization errors. It is believed that this error can be reduced by using a non-uniform discretization scheme without a significant increase in the computation time. Finally, this method can be easily extended to other types of planar transmission structures shown in Fig. 1.3.

5.4. Conclusion

It has been demonstrated that the time-domain method of lines is a reliable and efficient method which is capable of dealing with pulse propagation and scattering in discontinuity problems in planar trar smission lines. This is an extension of the two-dimensional results described in the previous chapters. It has been found that the DC-mode should be included in the modal field calculation to obtain correct results. The field can be described accurately by the proper placement of the discretized Ey field points near the edge of the microstrip line. Also, the frequency-domain characteristics obtained from the time-domain data have been made more stable by applying the QR

algorithm in the eigenmode calculation and by using the integrated field quantities in the extraction of frequency-domain parameters. The method can be applied to other planar structures.
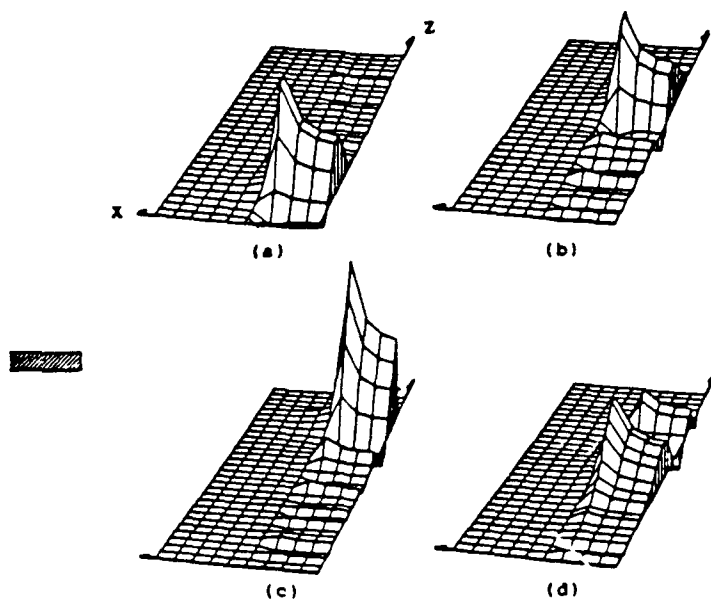
Fig.5.12 Ey configuration beneath a microstrip open-end discontinuity (a=2,b=10,

h=0.7, W=0.7 mm) (a) t=0, (b) t=80, (c) t=120 and (d) t=160 p-sec.
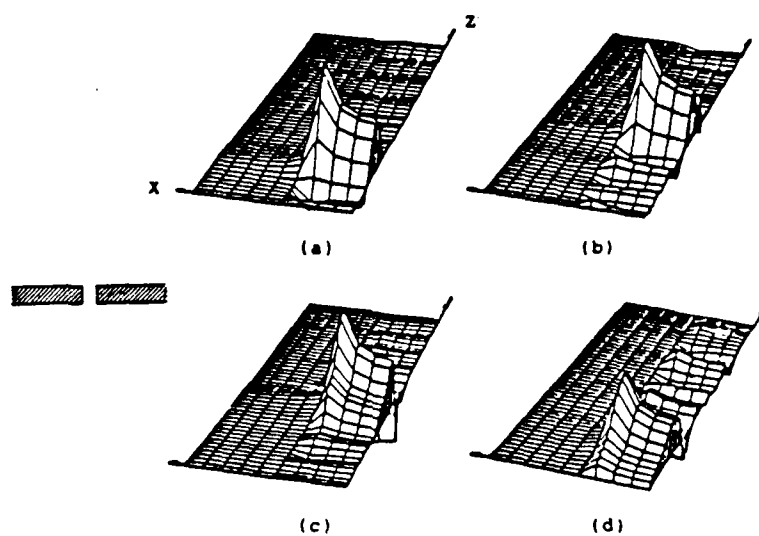

Fig. 5.13 Ey configuration beneath a microstrip gap discontinuity (a=2, b=10, h=0.7,

W=0.7, s=0.35 mm) (a) t=0, (b) t=40, (c) t=80 and (d) t=120 p-sec.
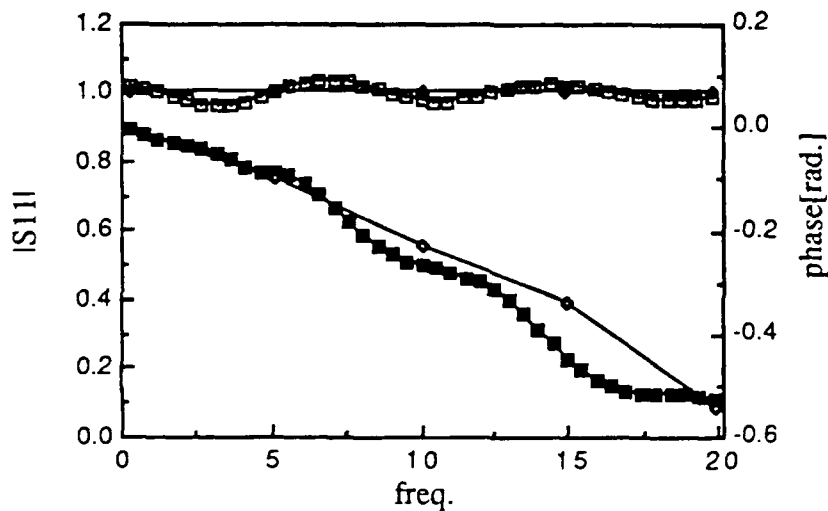
Fig.5.14 The magnitude and phase of S11 for the microstrip open-end
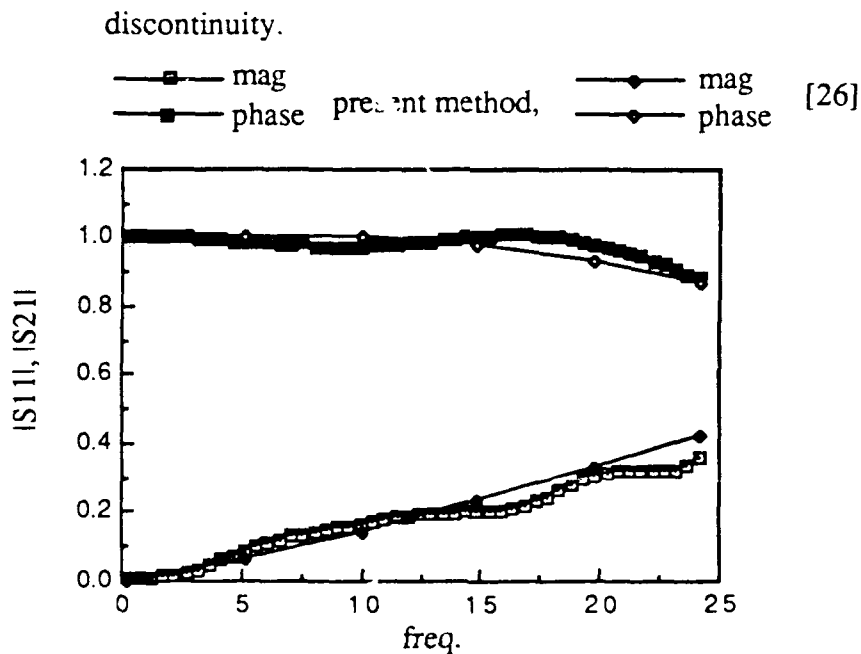
discontinuity.

Fig.5.15 Magnitude of S11 and S21 for a microstrip gap discontinuity

(ε r=9.6, h=0.7 mm, w/h=1, s/h=0.5)
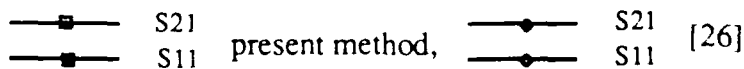
Chapter 6
Conclusion

6.1. Achievements

A new time-domain method, termed the Time-Domain Method of Lines, was proposed for the analysis of microwave and the millimeter-wave planar transmission lines and their associated discontinuities. This method makes use of the Method of Lines technique in solving the time-dependent Maxwell's equations. The unique structural feature of planar circuits, i.e., the space above and below the interfacing surface is uniform and homogeneous, can be incorporated. Therefore, three-dimensional structures are discretized only on the two-dimensional substrate surface and an analytical solution is used along the normal direction. Because of this semi-analytical property of the method, it has a number of potential advantages over many other time-domain methods. First, memory and computation time can be reduced since analytical processing is employed. Second, this method can handle an open boundary in the vertical (y) direction easily because of an analytical solution used in the y-direction.

With this new method, the accurate cutoff frequency spectra of a partially filled rectangular waveguide and a finned rectangular waveguide were found from the impulse response of the structures. Also, the method was extended to three-dimensional problems such as pulse propagation and scattering in planar transmission lines with discontinuities. The characteristic impedance and the propagation constant

68

for a microstrip line and the scattering parameters of its discontinuities (step-in-width, open-end and gap discontinuities) for a wide range of frequencies were obtained from the time-domain data.

6.2. Future work

In future research, the proposed method needs to be applied to the analysis of other discontinuities in many planar transmission line circuits. The radiation effect of a discontinuity can be analyzed by the solution of an open boundary problem in the y-direction by using the proposed method.

The method itself can also be modified to improve the accuracy of the results without a significant increse in the computation time. This is possible through the use of a non-uniform discretization scheme [33].

Since most of the computation time in this method is spent on the calculation of the eigenfrequencies and the corresponding eigenmodes, it is desirable to devise a scheme to avoid that calculation. The two-region approach is a candidate for a new scheme, where the original problem is divided into two regions (above and below the substarte surface) and solved in each region with the equivalent magnetic current source on the interface boundary [38]. For example, Fig. 6.1 shows the equivalent two-region problem, where the original inhomogeneous problem shown in Fig. 4.1 is divided into two homogeneous structures with equivalent source on the aperture region.

$$\vec{M} = \hat{n} \times \vec{E} \qquad (6.1)$$
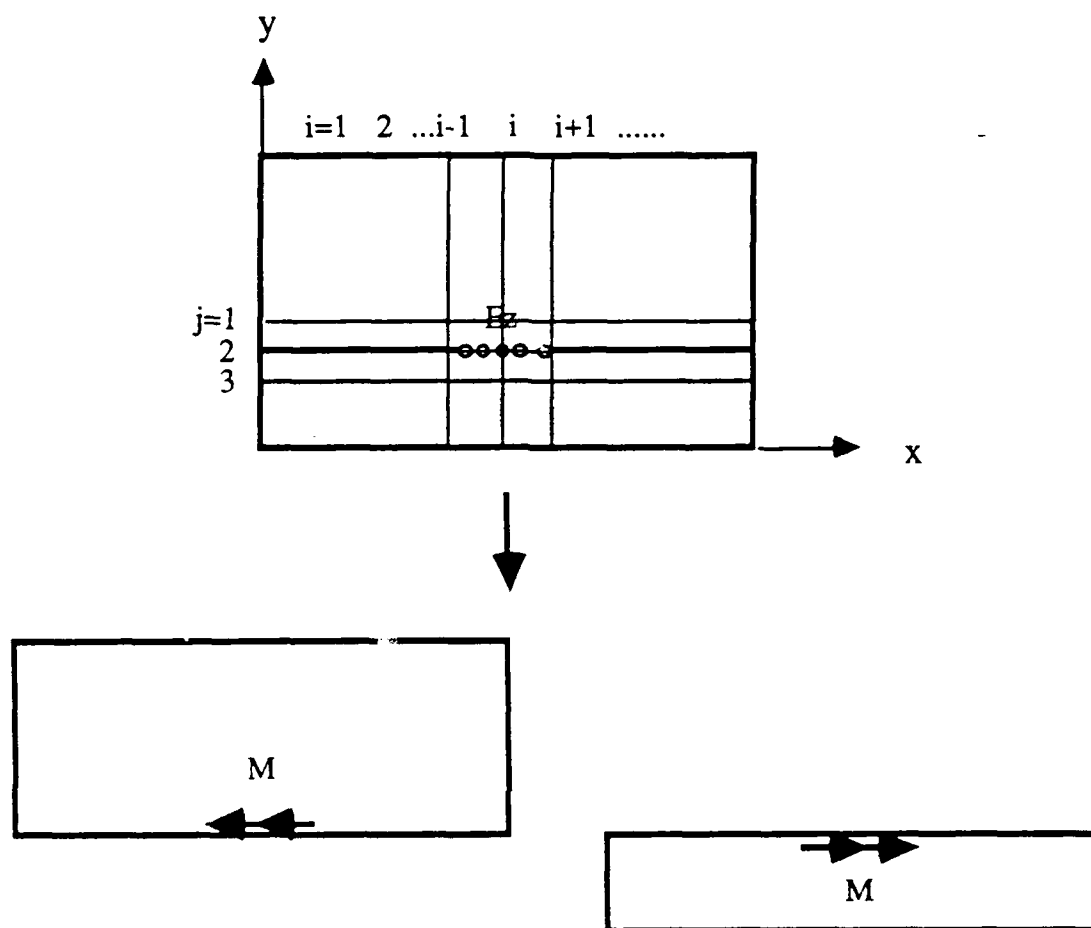
Fig. 6.1 An equivalent two-region problem of the probem considered in Chapter 4.

Also, Fig. 6.2 shows the another equivalent structure derived from Fig. 6.1 applying the image theorem [39]. Notice the structure 6.2 is a simple to solve because it is homegeneous and every discretized line is really independent each other so that the procedure described in the chapter 3 can be used. In this approach, the problem is to find the accurate equivalent magnetic current on the aperture at each time step. It can be obtained by applying the finite difference scheme around the aperture region in Fig. 6.1.
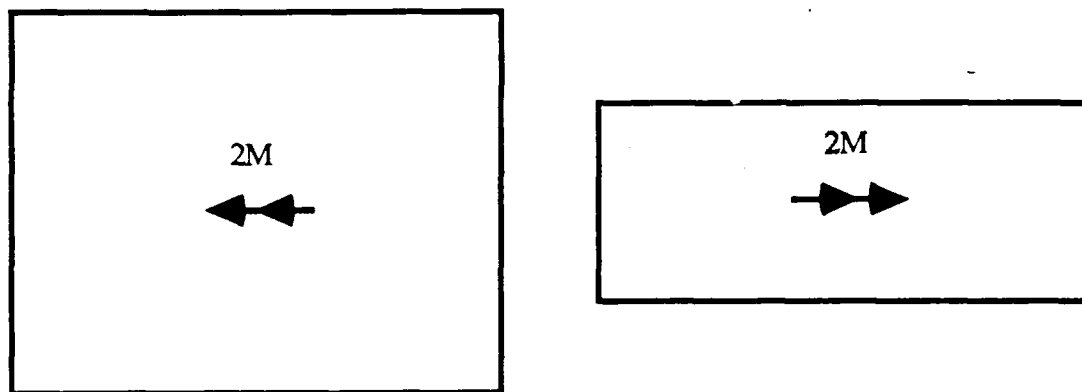
Fig. 6.2 An equivalent structure of Fig. 6.1 using the image theorem.

$$E_z^{N+1}(i,j) = 2E_z^N(i,j) - E_z^{N-1}(i,j)$$

$$+ \frac{c^2 \Delta t^2}{\Delta x^2}\left(E_z^N(i+1,j) - 2E_z^N(i,j) + E_z^N(i-1,j)\right)$$

$$+ \frac{c^2 \Delta t^2}{\Delta y^2}\left(E_z^N(i,j+1) - 2E_z^N(i,j) + E_z^N(i,j-1)\right)$$

(6.2)

where superscript N represents the N-th time step.

The difficulties encountered in this approach were in the representation of the pulse in terms of continuous basis functions on each line accurately and in the reproduction of original wave in terms of sampled pulses.

Appendix 1

Determination of the Eigenvalues and Eigenvectors of Second-Order Difference Matrix

The diagonalization matrix can be obtained from the eigenvectors belonging to the eigenvalues of the real symmetric matrix $[D_{xx}]$.

$$([D_{xx}] - \lambda_k^2 [I]) [X]_k = 0 \tag{A1.1}$$

where $[D_{xx}]$ is given by equation (2.14) and the subscript k means the k-th eigenvalue and eigenvector.

Since $[D_{xx}]$ is a tridiagonal matrix, equation (A1.1) actually represents N second-order difference equations

$$-X_{i-1}^{(k)} + (2 - \lambda_k^2) X_i^{(k)} - X_{i+1}^{(k)} = 0 , \quad i = 1, 2, ..., N \tag{A1.2}$$

where the subscript i means the i-th element of the k-th eigenvector.

Using the solution of the form,

$$X_i^{(k)} = A_k e^{ji\varphi_k} + B_k e^{-ji\varphi_k} \tag{A1.3}$$

the characteristic equation can be obtained from (A1.2), which has the characteristic root

$$\lambda_k^2 = 2 (1 - \cos \varphi_k) \tag{A1.4a}$$

or

$$\lambda_k^2 = 4 \sin^2 \varphi_k / 2 \tag{A1.4b}$$

72

where φ_k depends on the boundary conditions and are determined by using the boundary conditions shown in Table 2.1.

(i) Neumann - Dirichlet Condition

Assuming the number of the discretized lines is equal to N, the first and the last equation become

$$X_0(k) - X_1(k) = 0 \tag{A1.5a}$$

$$X_{N+1}(k) = 0 \tag{A1.5b}$$

or

$$\begin{bmatrix} 1 - e^{j\varphi_k} & 1 - e^{-j\varphi_k} \\ e^{j(N+1)\varphi_k} & e^{-j(N+1)\varphi_k} \end{bmatrix} \begin{bmatrix} A_k \\ B_k \end{bmatrix} = 0 \tag{A1.5c}$$

In order to have nontrivial solutions,

$$\varphi_k = \frac{k - 1/2}{N + 1/2} \pi, \quad k = 1, 2, \dots, N \tag{A1.6}$$

Using the first row of equation (A1.5) and the equation (A1.3),

$$(1 - e^{j\varphi_k}) A_k = - (1 - e^{-j\varphi_k}) B_k \tag{A1.7a}$$

$$e^{j\varphi_k/2} A_k = e^{-j\varphi_k/2} B_k \tag{A1.7b}$$

$$X_i^{(k)} = A_k \cos (i - 1/2) \varphi_k \tag{A1.8}$$

After normalization, the formula for the elements of the transformation matrix can be obtained.

$$T_{ND,ik} = \sqrt{\frac{2}{N+1/2}} \cos \frac{(i-1/2)(k-1/2)\pi}{N+1/2}, \quad i,k = 1,2,...,N \tag{A1.9}$$

(ii) Dirichlet - Neumann Condition

Assuming the number of the discretized lines is equal to N, the first and the last equation becomes

$$X_0(k) = 0 \tag{A1.10a}$$

$$- X_N(k) + X_{N+1}(k) = 0 \tag{A1.10b}$$

or

$$\begin{bmatrix} 1 & 1 \\ e^{jN\varphi_k}(e^{j\varphi_k}-1) & e^{-jN\varphi_k}(e^{-j\varphi_k}-1) \end{bmatrix} \begin{bmatrix} A_k \\ B_k \end{bmatrix} = 0 \tag{A1.10c}$$

In order to have nontrivial solutions,

$$\varphi_k = \frac{k-1/2}{N+1/2}\pi, \quad k = 1,2,...N \tag{A1.11}$$

Using the first row of equations (A1.10c) and (A1.3),

$$A_k = - B_k \tag{A1.12a}$$

$$X_i^{(k)} = A_k \sin i\, \varphi_k \tag{A1.12b}$$

After normalization, the formula for the elements of the transformation matrix can be obtained.

$$T_{ND,ik} = \sqrt{\frac{2}{N+1/2}} \sin \frac{i(k-1/2)\pi}{N+1/2}, \quad i,k = 1,2,...,N \tag{A1.13}$$

(iii) Dirichlet - Dirichlet Condition

Assuming the number of discretized lines is equal to N, the first and the last equation become

$$X_0^{(k)} = 0 \tag{A1.14a}$$

$$X_{N+1}^{(k)} = 0 \tag{A1.14b}$$

or

$$\begin{bmatrix} 1 & 1 \\ e^{j(N+1)\varphi_k} & e^{-j(N+1)\varphi_k} \end{bmatrix} \begin{bmatrix} A_k \\ B_k \end{bmatrix} = 0 \tag{A1.14c}$$

In order to have nontrivial solutions,

$$\varphi_k = \frac{k\pi}{N+1}, \quad k = 1, 2, \dots, N \tag{A1.15}$$

Using the first row of equations (A1.14c) and (A1.3),

$$A_k = -B_K \tag{A1.16}$$

$$X_i^{(k)} = A_k \sin i\,\varphi_k \tag{A1.17}$$

After normalization, the formula for the elements of the transformation matrix can be obtained.

$$T_{DD,ik} = \sqrt{\frac{2}{N+1}} \, \sin \frac{ik\pi}{N+1}, \quad i, k = 1, 2, \dots, N \tag{A1.18}$$

(iv) Neumann - Neumann Condition

Assuming the number of the discretized lines is equal to N+1 to be consistant with the D-D case, the first and the last equation become

$$X_0^{(k)} - X_1^{(k)} = 0 \tag{A1.19a}$$

$$X_{N+2}^{(k)} - X_{N+1}^{(k)} = 0 \tag{A1.19b}$$

or

$$\begin{bmatrix} 1 & 1 \\ e^{j(N+1)\varphi_k} & e^{-j(N+1)\varphi_k} \end{bmatrix} \begin{bmatrix} (1 - e^{j\varphi_k}) A_k \\ (1 - e^{-j\varphi_k}) B_k \end{bmatrix} = 0 \tag{A1.19c}$$

In order to have nontrivial solutions,

$$\varphi_k = \frac{k \pi}{N+1}, \quad k = 0, 1, 2, \ldots, N \tag{A1.20}$$

Using the first row of equations (A1.19c) and (A1.20),

$$(1 - e^{j\varphi_k}) A_k = -(1 - e^{-j\varphi_k}) B_k \tag{A1.21a}$$

$$e^{j\varphi_k/2} A_k = e^{-j\varphi_k/2} B_k \tag{A1.21b}$$

$$X_i^{(k)} = A_k \cos(i - 1/2) \varphi_k \tag{A1.22}$$

After normalization, the formula for the elements of the transformation matrix can be obtained.

$$T_{NN,i1} = \sqrt{\frac{1}{N+1}}$$

$$T_{NN,i\,k+1} = \sqrt{\frac{2}{N+1}} \cos \frac{(i - 1/2) k \pi}{N+1}, \quad i = 1, 2, \ldots, N+1, k = 1, 2, \ldots, N \tag{A1.23}$$

Appendix 2

Calculation of the Quasi-Diagonal Matrices $[d_x]$ of the First-Order Difference Operator $[D_x]$

The matrix $[d_x]$ is defined as a product of the first-order difference matrix $[D_x]$ with the corresponding transformation matrix $[T_x]$ from the right and with the transposed matrix $[T_x^d]^t$ of the dual boundary value problem from the left.

$$[d_x] = [T_x^d]^t [D_x] [T_x] \qquad (A2.1)$$

where the superscript 'd' denotes the dual boundary condition. Before $[d_x]$ is determined, one result may be anticipated. The eigenvalue matrix $[\lambda^2]$ results from the product

$$[d_x]^t [d_x] = [T_x]^t [D_x]^t [T_x^d \, {}^r T_x^d]^t [D_x] [T_x] = [T_x]^t [D_x]^t [D_x] [T_x] = [\lambda^2]$$

$$(A2.2)$$

where the equations (2.16) and (2.14) are used. Therefore, the relation between $[d_x]$ and $[\lambda^2]$ is anticipated.

(i) Boundary Conditions DD and NN

For the boundary condition DD, the first-order difference matrix $[D_x^{DD}]$ is given in Table 2.2. The corresponding $[d_x^{DD}]$ is

$$[d_x^{DD}] = [T_x^{NN}]^t [D_x^{DD}] [T_x^{DD}] \qquad (A2.3)$$

77

If we multiply $[T_X^{NN}]^t$ by $[D_X^{DD}]$, we find that the first row of the result vanishes because all the elements of the first column vector in $[T_X^{NN}]$ are the same. The remaining part of the resulting matrix can be written as a product of $[\lambda_{DD}]$ and $[T_X^{DD}]$, where $[\lambda_{DD}]$ is the diagonal matrix formed by the positive square roots of $[\lambda_{DD}{}^2]$. Therefore,

$$\left[T_x^{NN}\right]^t \left[D_x\right] = \begin{bmatrix} 0 \\ \left[\lambda_{DD}\right]\left[T_x^{DD}\right] \end{bmatrix} = \begin{bmatrix} 0 \\ \left[\lambda_{DD}\right] \end{bmatrix}\begin{bmatrix} T_x^{DD} \end{bmatrix}$$

(A2.4)

Since $[T_X^{DD}]$ is a symmetric matrix, $[T_X^{DD}] = [T_X^{DD}]^t$. Consequently $[d_X^{DD}]$ is given by

$$\left[d_x^{DD}\right] = \begin{bmatrix} 0 \\ \left[\lambda_{DD}\right] \end{bmatrix}$$

(A2.5)

Thus $[d_X^{DD}]$ is a quasidiagonal matrix.

Using the equation (2.5), it can be shown easily that

$$[d_X^{NN}] = - [d_X^{DD}]$$

(A2.6)

for the boundary condition NN.

(ii) Boundary Condition DN and ND

For the boundary condition DN, the first-order difference matrix is given in Table 2.2. In that case, the corresponding $[d_X^{DN}]$ is given by

$$[d_X^{DN}] = [T_X^{ND}]^t [D_X^{DN}] [T_X^{DN}]$$

(A2.7)

Using the procedure described previously, we can find that

$$[d_x{}^{DN}] = [\lambda_{DN}] = [d_x{}^{ND}] \qquad (A2.8)$$

where the k-th diagonal element of $[\lambda_{DN}]$, λ_k, is given by the positive root of $\lambda_k{}^2$.

Appendix 3

Calculation of Modal fields in three-dimensional problems

(I) Time-Harmonic Case

In three-dimensional problems shown in Fig. 5.1, all the six field components should be considered to satisfy the boundary conditions. Usually, two scalar potentials, $\Psi^e(x,y,z,t)$ and $\Psi^h(x,y,z,t)$, are introduced to simplify the formulation instead of considering all six field components. The fields can be derived from the solution of two scalar potentials. The equations for the potentials are given by

$$\partial^2 \Psi^e / \partial x^2 + \partial^2 \Psi^e / \partial y^2 + \partial^2 \Psi^e / \partial z^2 - \partial^2 \Psi^e / \partial t^2 = 0 \qquad (A3.1a)$$

$$\partial^2 \Psi^h / \partial x^2 + \partial^2 \Psi^h / \partial y^2 + \partial^2 \Psi^h / \partial z^2 - \partial^2 \Psi^h / \partial t^2 = 0 \qquad (A3.1b)$$

Using the separation of variables technique, $\Psi(x,y,z,t) = \psi(x,y,z)\, T(t)$, the time-dependent solution is of the form

$$T(t) = A \cos(\omega t) + B \sin(\omega t). \qquad (A3.2)$$

The space-dependent equations are given by

$$\partial^2 \psi^e / \partial x^2 + \partial^2 \psi^e / \partial y^2 + \partial^2 \psi^e / \partial z^2 + \omega^2 \mu \varepsilon(y)\, \psi^e = 0 \qquad (A3.3a)$$

$$\partial^2 \psi^h / \partial x^2 + \partial^2 \psi^h / \partial y^2 + \partial^2 \psi^h / \partial z^2 + \omega^2 \mu \varepsilon(y)\, \psi^h = 0 \qquad (A3.3b)$$

with the boundary conditions,

80

$$\psi^e(x,y,z) = 0, \text{ at } y = 0, b \qquad (A3.4a)$$

$$\partial \psi^h(x,y,z) / \partial y = 0, \text{ at } y = 0, b \qquad (A3.4b)$$

At y = h,

$$E_{xI} - E_{xII} = \frac{\partial^2 \psi_I^e}{j\omega\varepsilon_r\varepsilon_0 \partial x\,\partial z} - \frac{\partial \psi_I^h}{\partial y} - \frac{\partial^2 \psi_{II}^e}{j\omega\varepsilon_0 \partial x\,\partial z} + \frac{\partial \psi_{II}^h}{\partial y} = 0 \qquad (A3.4c)$$

$$E_{zI} - E_{zII} = \frac{1}{j\omega\varepsilon_r\varepsilon_0} (\frac{\partial^2}{\partial z^2} + \varepsilon_r \omega^2 \mu_0\varepsilon_0) \psi_I^e - \frac{1}{j\omega\varepsilon_0}(\frac{\partial^2}{\partial z^2} + \omega^2 \mu_0\varepsilon_0) \psi_{II}^e = 0 \qquad (A3.4d)$$

$$H_{xI} - H_{xII} = \frac{1}{j\omega\mu_0} \frac{\partial^2 \psi_I^h}{\partial x\,\partial z} + \frac{\partial \psi_I^e}{\partial y} - \frac{1}{j\omega\mu_0} \frac{\partial^2 \psi_{II}^h}{\partial x\,\partial z} - \frac{\partial \psi_{II}^e}{\partial y} = -J_z \qquad (A3.4e)$$

$$H_{zI} - H_{zII} = \frac{1}{j\omega\mu_0} (\frac{\partial^2}{\partial z^2} + \omega^2 \mu_0\varepsilon_r\varepsilon_0) \psi_I^h - \frac{1}{j\omega\mu_0} (\frac{\partial^2}{\partial z^2} + \omega^2 \mu_0\varepsilon_0) \psi_{II}^h = J_x \qquad (A3.4f)$$

where subscripts I, II represent the regions shown in Fig. 5.1.

The first step of analysis is the discretization of the equation according to the rule explained in Chapter 2, which gives

$$\frac{\partial^2 \left[\psi^e\right]}{\partial y^2} + \frac{\left[D_{xx}^{ND}\right]\left[\psi^e\right]}{\Delta x^2} + \frac{\left[\psi^e\right]\left[D_{xx}^{ND}\right]^t}{\Delta z^2} + \omega^2 \mu_c(y)\left[\psi^e\right] = \left[0\right] \qquad (A3.5a)$$

$$\frac{\partial^2 \left[\psi^h\right]}{\partial y^2} + \frac{\left[D_{xx}^{DN}\right]\left[\psi^h\right]}{\Delta x^2} + \frac{\left[\psi^h\right]\left[D_{xx}^{DN}\right]^t}{\Delta z^2} + \omega^2 \mu \varepsilon(y)\left[\psi^h\right] = [0]$$

(A3.5b)

with the boundary conditions

$[\psi^e] = 0$, at $y = 0, b$

(A3.6a)

$\partial[\psi^h] / \partial y = 0$, at $y = 0, b$

(A3.6b)

At $y = h$,

$$\frac{1}{j\omega\varepsilon_r\varepsilon_0} \frac{\left[D_x^{ND}\right]\left[\psi_I^e\right]\left[D_z^{ND}\right]^t}{\Delta x \, \Delta z} - \frac{\partial\left[\psi_I^h\right]}{\partial y} - \frac{1}{j\omega\varepsilon_0} \frac{\left[D_x^{ND}\right]\left[\psi_{II}^e\right]\left[D_z^{ND}\right]^t}{\Delta x \, \Delta z} + \frac{\partial\left[\psi_{II}^h\right]}{\partial y} = [0]$$

(A3.6c)

$$\frac{1}{j\omega\varepsilon_r\varepsilon_0}\left(\frac{\left[\psi_I^e\right]\left[D_{zz}^{ND}\right]^t}{\Delta z^2} + \varepsilon_r\omega^2\mu_0\varepsilon_0\left[\psi_I^e\right]\right) - \frac{1}{j\omega\varepsilon_0}\left(\frac{\left[\psi_{II}^e\right]\left[D_{zz}^{ND}\right]^t}{\Delta z^2} + \omega^2\mu_0\varepsilon_0\left[\psi_{II}^e\right]\right) = [0]$$

(A3.6d)

$$\frac{1}{j\omega\mu_0} \frac{\left[D_x^{ND}\right]^t\left[\psi_I^h\right]\left[D_z^{ND}\right]}{\Delta x \, \Delta z} + \frac{\partial\left[\psi_I^e\right]}{\partial y} - \frac{1}{j\omega\mu_0} \frac{\left[D_x^{ND}\right]^t\left[\psi_{II}^h\right]\left[D_z^{ND}\right]}{\Delta x \, \Delta z} - \frac{\partial\left[\psi_{II}^e\right]}{\partial y} = -[J_z]$$

(A3.6e)

$$\frac{1}{j\omega\mu_0}\left(\frac{\left[\psi_I^h\right]\left[D_{zz}^{DN}\right]^t}{\Delta z^2} + \varepsilon_r\omega^2\mu_0\varepsilon_0\left[\psi_I^h\right]\right) - \frac{1}{j\omega\mu_0}\left(\frac{\left[\psi_{II}^h\right]\left[D_{zz}^{DN}\right]^t}{\Delta z^2} + \omega^2\mu_0\varepsilon_0\left[\psi_{II}^h\right]\right) = [J_x]$$

(A3.6f)

Since the matrices $[D_{xx}^{ND}]$, $[D_{xx}^{DN}]$, $[D_{zz}^{ND}]$, and $[D_{zz}^{DN}]$ are real

symmetric matrices, they can be diagonalized by appropriate transformation matrices

(see Table 2.3). The potentials can also be transformed into the "transformed potentials",

$$[U] = [T_x^{ND}]^t \, [\psi^e] \, [T_z^{ND}]$$ (A3.7a)

$$[V] = [T_x^{DN}]^t \, [\psi^h] \, [T_z^{DN}]$$ (A3.7b)

Then, equations (A3.6a,b) are transformed into

$$\frac{\partial^2 [U]}{\partial y^2} + \frac{[d_{xx}^{ND}][U]}{\Delta x^2} + \frac{[U][d_{zz}^{ND}]^t}{\Delta z^2} + \omega^2 \mu \varepsilon(y) [U] = [0]$$ (A3.8a)

$$\frac{\partial^2 [V]}{\partial y^2} + \frac{[d_{xx}^{DN}][V]}{\Delta x^2} + \frac{[V][d_{zz}^{DN}]^t}{\Delta z^2} + \omega^2 \mu \varepsilon(y) [V] = [0]$$ (A3.8b)

with the transformed boundary conditions,

$$[U] = 0, \text{ at } y = 0, b$$ (A3.9a)

$$\partial [V] / \partial y = 0, \text{ at } y = 0, b$$ (A3.9b)

At y = h,

$$\frac{1}{j\omega \varepsilon_r \varepsilon_0} \frac{[d_x^{ND}][U_I][d_z^{ND}]^t}{\Delta x \, \Delta z} - \frac{\partial [V_I]}{\partial y} - \frac{1}{j\omega \varepsilon_0} \frac{[d_x^{ND}][U_{II}][d_z^{ND}]^t}{\Delta x \, \Delta z} + \frac{\partial [V_{II}]}{\partial y} = [0]$$ (A3.9c)

$$\frac{1}{j\omega \varepsilon_r \varepsilon_0} \left(\frac{[U_I][d_{zz}^{ND}]^t}{\Delta z^2} + \omega^2 \mu_0 \varepsilon_r \varepsilon_0 [U_I] \right) - \frac{1}{j\omega \varepsilon_0} \left(\frac{[U_{II}][d_{zz}^{ND}]^t}{\Delta z^2} + \omega^2 \mu_0 \varepsilon_0 [U_{II}] \right) = [0]$$ (A3.9d)

8 4

$$\frac{1}{j\omega\mu_0}\frac{\left[d_x^{ND}\right]^t[V_I]\left[d_z^{ND}\right]}{\Delta x\,\Delta z}+\frac{\partial[U_I]}{\partial y}-\frac{1}{j\omega\mu_0}\frac{\left[d_x^{ND}\right]^t[V_{II}]\left[d_z^{ND}\right]}{\Delta x\,\Delta z}-\frac{\partial[U_{II}]}{\partial y}=-\left[\tilde{J}_z\right]$$

(A3.9e)

$$\frac{1}{j\omega\mu_0}(\frac{[V_I]\left[d_{zz}^{DN}\right]^t}{\Delta z^2}+\omega^2\mu_0\varepsilon_r\varepsilon_d[V_I])-\frac{1}{j\omega\mu_0}(\frac{[V_{II}]\left[d_{zz}^{DN}\right]^t}{\Delta z^2}+\omega^2\mu_0\varepsilon_d[V_{II}])=\left[\tilde{J}_x\right]$$

(A3.9f)

Now equations (A3.8a,b) are uncoupled so that the general solution of the ik-th line which satisfies the boundary condition (A3.8a,b) can be obtained

$$U_{I,ik}=A_{I,ik}\sinh\kappa_{I,ik}y$$ (A3.10a)

$$U_{II,ik}=A_{II,ik}\sinh\kappa_{II,ik}(b-y)$$ (A3.10b)

$$V_{I,ik}=B_{I,ik}\cosh\eta_{I,ik}y$$ (A3.10c)

$$V_{II,ik}=B_{II,ik}\cosh\eta_{II,ik}(b-y)$$ (A3.10d)

where

$$\kappa_{I,ik}^2=-[d_{xx,i}^{ND}/\Delta x^2+d_{zz,k}^{ND}/\Delta z^2+\omega^2\mu\varepsilon_r\varepsilon_0]$$ (A3.11a)

$$\kappa_{II,ik}^2=-[d_{xx,i}^{ND}/\Delta x^2+d_{zz,k}^{ND}/\Delta z^2+\omega^2\mu\varepsilon_0]$$ (A3.11b)

$$\eta_{I,ik}^2=-[d_{xx,i}^{DN}/\Delta x^2+d_{zz,k}^{DN}/\Delta z^2+\omega^2\mu\varepsilon_r\varepsilon_0]$$ (A3.11c)

$$\eta_{II,ik}^2=-[d_{xx,i}^{DN}/\Delta x^2+d_{zz,k}^{DN}/\Delta z^2+\omega^2\mu\varepsilon_0]$$ (A3.11d)

By means of these solutions, the derivatives of U and V with respect to y at y = h can be represented by the values of U and V at y = h.

$$\frac{dU_{I,ik}}{dy}=\frac{\kappa_{I,ik}}{\tanh\kappa_{I,ik}h}U_{I,ik}\quad,\text{ at }y=h$$ (A3.12a)

$$\frac{dU_{II,ik}}{dy}=-\frac{\kappa_{II,ik}}{\tanh\kappa_{II,ik}d}U_{II,ik}\quad,\text{ at }y=h$$ (A3.12a)

$$\frac{dV_{I,ik}}{dy} = \eta_{I,ik}\tanh \eta_{I,ik} h\, V_{I,ik} \text{, at } y = h \tag{A3.12a}$$

$$\frac{dV_{II,ik}}{dy} = -\eta_{I,ik}\tanh \eta_{I,ik} d\, V_{II,ik} \text{, at } y = h \tag{A3.12a}$$

Now the equations (A3.9c~f) have six unknowns $U_{I,ik}$, $U_{II,ik}$, $V_{I,ik}$, $V_{II,ik}$, $J_{x,ik}$ and $J_{z,ik}$ at $y = h$. Therefore, the continuity equations in (A3.9c~f) can be used to solve for the potentials, $U_{I,ik}$, $U_{II,ik}$, $V_{I,ik}$ and $V_{II,ik}$ at $y = h$ in terms of the current densities, $J_{x,ik}$ and $J_{z,ik}$.

$$\begin{bmatrix} U_I \\ V_I \end{bmatrix}_{ik} = \frac{1}{c_{11}c_{22} - c_{12}c_{21}} \begin{bmatrix} c_{22}b_1 - c_{12}b_2 & c_{12} \\ c_{11}b_2 - c_{21}b_1 & -c_{11} \end{bmatrix} \begin{bmatrix} \widetilde{J}_x \\ \widetilde{J}_z \end{bmatrix}_{ik} \tag{A3.13a}$$

where

$$c_{11} = \frac{1}{j\omega\varepsilon_r\varepsilon_0} \frac{d_{x,i}d_{z,k}}{\Delta x\, \Delta z} \left(1 - \frac{\dfrac{d_{zz,k}^{ND}}{2} + \omega^2\mu_0\varepsilon_r\varepsilon_0}{\dfrac{d_{zz,k}^{ND}}{2} + \omega^2\mu_0\varepsilon_0} \right) \tag{A3.13b}$$

$$c_{12} = -\eta_{I,ik}\tanh \eta_{I,ik} h - \eta_{II,ik}\tanh \eta_{II,ik} d \left(\frac{\dfrac{d_{zz,k}^{DN}}{2} + \omega^2\mu_0\varepsilon_r\varepsilon_0}{\dfrac{d_{zz,k}^{DN}}{2} + \omega^2\mu_0\varepsilon_0} \right) \tag{A3.13c}$$

$$c_{21} = \kappa_{I,ik} \coth \kappa_{I,ik} h + \kappa_{II,ik} \coth \kappa_{II,ik} d \left(\frac{\dfrac{d_{zz,k}^{ND}}{\Delta z^2} + \omega^2 \mu_0 \varepsilon_r \varepsilon_0}{\varepsilon_r (\dfrac{d_{zz,k}^{ND}}{\Delta z^2} + \omega^2 \mu_0 \varepsilon_0)} \right)$$

(A3.13d)

$$c_{22} = \frac{1}{j\omega\mu_0} \frac{d_{x,i}^{DN} d_{z,k}^{DN}}{\Delta x \, \Delta z} \left(1 - \frac{\dfrac{d_{zz,k}^{DN}}{\Delta z^2} + \omega^2 \mu_0 \varepsilon_r \varepsilon_0}{\dfrac{d_{zz,k}^{DN}}{\Delta z^2} + \omega^2 \mu_0 \varepsilon_0} \right)$$

(A3.13e)

$$b_1 = - j\omega\mu_0 \, \eta_{II,ik} \tanh \eta_{II,ik} d \, \frac{1}{\dfrac{d_{zz,k}^{DN}}{\Delta z^2} + \omega^2 \mu_0 \varepsilon_0}$$

(A3.13f)

$$b_2 = - \frac{d_{x,i}^{DN} d_{z,k}^{DN}}{\Delta x \, \Delta z} \, \frac{1}{\dfrac{d_{zz,k}^{DN}}{\Delta z^2} + \omega^2 \mu_0 \varepsilon_0}$$

(A3.13g)

Then, the field values at y = h can be found by using the following relations evaluated at y = h.

$$\widetilde{E_{x,ik}}(y) = \frac{1}{j\omega\varepsilon(y)} \frac{d_{x,i}^{ND} d_{z,k}^{ND}}{\Delta x \, \Delta z} U_{ik}(y) - \eta_{ik} \tanh \eta_{ik} h \, V_{ik}(y)$$

(A3.14a)

$$\widetilde{E_{y,ik}}(y) = \frac{1}{j\omega\varepsilon(y)} \frac{d_{z,k}^{ND}}{\Delta z} \frac{\partial}{\partial y} U_{ik}(y) - \frac{d_{x,i}^{DN}}{\Delta x} V_{ik}(y)$$

(A3.14b)

$$\widetilde{E_{z,ik}}(y) = \frac{1}{j\omega\varepsilon(y)} (\frac{d_{zz,k}^{ND}}{\Delta z^2} + \omega^2 \mu\varepsilon(y)) \, U_{ik}(y)$$

(A3.14c)

$$\widetilde{H_{x,ik}}(y) = \frac{\kappa_{ik}}{\tanh \kappa_{ik} h} U_{ik}(y) + \frac{1}{j\omega\mu_0} \frac{d_{x,i}^{DN} d_{z,k}^{DN}}{\Delta x \, \Delta z} V_{ik}(y)$$

(A3.14d)

$$\widetilde{H_{y,ik}}(y) = -\frac{d_{x,i}^{ND}}{\Delta x} U_{ik}(y) + \frac{1}{j\omega\mu_0} \frac{d_{z,k}^{DN}}{\Delta z} \frac{\partial}{\partial y} V_{ik}(y)$$

(A3.14e)

$$\widetilde{H_{z,ik}}(y) = \frac{1}{j\omega\mu_0} \left(\frac{d_{zz,k}^{DN}}{\Delta z^2} + \omega^2 \mu\varepsilon(y) \right) V_{ik}(y)$$

(A3.14f)

From this point on, we change the two-dimensional arrays for fields and currents into one-dimensional arrays for convinience of formulation according to the rule

$$n = i + (k - 1) N_x \, , \; 1 < i < N_x, \; 1 < k < N_z$$

(A3.15)

Then, the two-dimensional N_x by N_z matrices become $N_x N_z$ column matrices and equations (A3.14a,b) can be expressed in the following form:

$$\begin{bmatrix} \widetilde{E}_z \\ \widetilde{E}_x \end{bmatrix} = \begin{bmatrix} [\widetilde{Z_{zz}}] & [\widetilde{Z_{zx}}] \\ [\widetilde{Z_{xz}}] & [\widetilde{Z_{xx}}] \end{bmatrix} \begin{bmatrix} \widetilde{J}_z \\ \widetilde{J}_x \end{bmatrix}$$

(A3.16)

where [Z]'s are diagonal matrices.

Before the final boundary condition is applied, a useful matrix operation, the Kronecker product, is introduced

$$[A] \otimes [B] = \begin{bmatrix} a_{11}[B] & . & . & a_{1n}[B] \\ . & & & . \\ . & & & . \\ a_{m1}[B] & . & . & a_{mn}[B] \end{bmatrix}$$

(A3.17)

Two important properties of the Kronecker product are

$$([A] \otimes [B]) ([C] \otimes [D]) = ([A] [C]) \otimes ([B] [D])$$ - (A3.18a)

$$([A] \otimes [B])^t = [A]^t \otimes [B]^t$$ (A3.18b)

Now, the final boundary condition is that the tangential electric fields should be zero on the metalization part of the substrate surface. In order to apply this condition, we have to go back to the original domain using the inverse transformation relation

$$[E_z]_{2D} = \left[T_x^{ND} \right] \left[\widetilde{E_z} \right]_{2D} \left[T_z^{ND} \right]^t \longrightarrow [E_z] = (\left[T_z^{ND} \right] \otimes \left[T_x^{ND} \right]) \left[\widetilde{E_z} \right]$$ (A3.19a)

$$[E_x]_{2D} = \left[T_x^{DN} \right] \left[\widetilde{E_x} \right]_{2D} \left[T_z^{DN} \right]^t \longrightarrow [E_x] = (\left[T_z^{DN} \right] \otimes \left[T_x^{DN} \right]) \left[\widetilde{E_x} \right]$$ (A3.19b)

$$[J_z]_{2D} = \left[T_x^{ND} \right] \left[\widetilde{J_z} \right]_{2D} \left[T_z^{ND} \right]^t \longrightarrow [J_z] = (\left[T_z^{ND} \right] \otimes \left[T_x^{ND} \right]) \left[\widetilde{J_z} \right]$$ (A3.19c)

$$[J_x]_{2D} = \left[T_x^{DN} \right] \left[\widetilde{J_x} \right]_{2D} \left[T_z^{DN} \right]^t \longrightarrow [J_x] = (\left[T_z^{DN} \right] \otimes \left[T_x^{DN} \right]) \left[\widetilde{J_x} \right]$$ (A3.19d)

where the subscript 2D means the two-dimensional matrix considered up to equation (A3.14). The equation (3.15) can be inverse transformed into

$$\begin{bmatrix} E_z \\ E_x \end{bmatrix}_{red} = \begin{bmatrix} [Z_{zz}][Z_{zx}] \\ [Z_{xz}][Z_{xx}] \end{bmatrix}_{red} \begin{bmatrix} J_z \\ J_x \end{bmatrix}_{red} = [0]$$ (A3.20)

where 'red' represents the reduced matrix made by deleting the rows and columns corresponding to the non-metalization lines from the full matrix. Equation (A3.20) will have nontrivial solutions at the resonant frequencies of the structure only. The resonant frequencies are found from the determinant equation

$$\det \begin{bmatrix} [Z_{zz}] & [Z_{zx}] \\ [Z_{xz}] & [Z_{xx}] \end{bmatrix}_{red} = [0] \tag{A3.21}$$

At resonance, the modal current distribution can be found as an eigenvector in (A3.20) by using the QR algorithm for the stability of the solution.

One inportant thing to be mentioned in the calculation of the roots is the elimination of poles present in the matrix element in order to obtain the correct roots. One way to remove the poles in the determinant calculation is by the pole multiplication method, in which all the elements are multiplied by the common dinominator. In this case, the pole extraction is performed in equation (A3.16), not in equation (A3.21). This is because the poles in equation (A3.16) can be easily found. The process is as follows:

$$\begin{bmatrix} \dfrac{N_1}{D_1} & \\ & \cdot \\ & & \dfrac{N_1}{D_1} \end{bmatrix} = \dfrac{1}{\displaystyle\prod_{i=1}^{N} D_i} \begin{bmatrix} N_1 \overline{D_1} & \\ & \cdot \\ & & N_N \overline{D_N} \end{bmatrix} \tag{A3.22a}$$

where

$$\overline{D_i} = \prod_{i=1, i \neq i}^{N} D_j \tag{A3.22b}$$

After the values of the potentials, $U_{I,ik}$, $U_{II,ik}$, $V_{I,ik}$, $V_{II,ik}$ at $y = h$ are known from the modal current density distribution obtained in the previous step, the coefficients $A_{I,ik}$, $B_{I,ik}$, $A_{II,ik}$ and $B_{II,ik}$ in equations (A3.10a~d) can be determined. Therefore, the transformed modal fields of the given structure can be obtained by equations (A3.14a~f).

(II) Static Case

In this case, the governing equation is the Laplace's equation with proper boundary conditions:

$$\nabla^2 V = 0 \tag{A3.23}$$

and at $y = h$,

$$E_{xI} - E_{xII} = -\frac{\partial V_I}{\partial x} + \frac{\partial V_{II}}{\partial x} = 0 \tag{A3.24a}$$

$$E_{zI} - E_{zII} = -\frac{\partial V_I}{\partial z} + \frac{\partial V_{II}}{\partial z} = 0 \tag{A3.24b}$$

$$\varepsilon_r E_{yI} - E_{yII} = -\varepsilon_r \frac{\partial V_I}{\partial y} + \frac{\partial V_{II}}{\partial z} = -\rho \tag{A3.24c}$$

where the subscripts I and II represent the regions shown in Fig. 5.1.

Using the discretization rule described in Chapter 2, equations (A3.23) and (A3.24a~c) can be discretized as follows :

$$\frac{\partial}{\partial y^2}[V] + \frac{1}{\Delta x^2}\left[D_{xx}^{ND}\right][V] + \frac{1}{\Delta z^2}[V]\left[D_{zz}^{DN}\right]^t = 0 \tag{A3.25}$$

at $y = h$

$$-\frac{1}{\Delta x}\left[D_x^{ND}\right][V_I] + \frac{1}{\Delta x}\left[D_x^{ND}\right][V_{II}] = 0 \tag{A3.26a}$$

$$\frac{1}{\Delta z}[V_I]\left[D_z^{DN}\right]^t - \frac{1}{\Delta z}[V_{II}]\left[D_z^{DN}\right]^t = 0 \tag{A3.26b}$$

$$- \varepsilon_r \frac{\partial}{\partial y} [V_I] + \frac{\partial}{\partial y} [V_{II}] = - [\rho]$$

<div align="right">(A3.26c)</div>

where [ ] represents a matrix whose ij-th element represents the potential at the ij-th line.

Since the second-order difference matries $[D_{xx}^{ND}]$ and $[D_{zz}^{DN}]$ are real symmetirc matrices, they can be diagonalized by using the transformation matries (see Table 2.3)

$$[T_x^{ND}]^t [D_{xx}^{ND}] [T_x^{ND}] = \text{diag} [d_{xx}^{ND}]$$

<div align="right">(A3.27a)</div>

$$[T_z^{DN}]^t [D_{zz}^{DN}] [T_z^{DN}] = \text{diag} [d_{zz}^{DN}]$$

<div align="right">(A3.27b)</div>

The potential [V] is also transformed into a transformed potential [U],

$$[U] = [T_x^{ND}]^t [V] [T_z^{DN}]$$

<div align="right">(A3.28)</div>

Then, equations (A3.23) and (A3.24a~c) become

$$\frac{\partial}{\partial y^2} [U] + \frac{1}{\Delta x^2} [d_{xx}^{ND}] [U] + \frac{1}{\Delta z^2} [U] [d_{zz}^{DN}]^t = 0$$

<div align="right">(A3.29)</div>

at y = h

$$- \frac{1}{\Delta x} [d_x^{ND}] [U_I] + \frac{1}{\Delta x} [d_x^{ND}] [U_{II}] = 0$$

<div align="right">(A3.30a)</div>

$$\frac{1}{\Delta z} [U_I] [d_z^{DN}] - \frac{1}{\Delta z} [U_{II}] [d_z^{DN}] = 0$$

<div align="right">(A3.30b)</div>

$$- \varepsilon_r \frac{\partial}{\partial y} [U_I] + \frac{\partial}{\partial y} [U_{II}] = - [\tilde{\rho}]$$

<div align="right">(A3.30c)</div>

The solution of equation (A3.29) which satisfies the top and bottom boundary condition can be written as

$$U_{I,ik} = A_{I,ik} \frac{\sinh \kappa_{ik} y}{\kappa_{ik}} \quad , \text{ in region I} \qquad (A3.31a)$$

$$U_{II,ik} = A_{II,ik} \frac{\sinh \kappa_{ik}(b-y)}{\kappa_{ik}} \quad , \text{ in region II} \qquad (A3.31b)$$

where

$$\kappa_{ik}^2 = -\frac{d_{xx,i}^{ND}}{\Delta x^2} - \frac{d_{zz,k}^{DN}}{\Delta z^2} \qquad (A3.31c)$$

By means of these solutions, the derivative of the potentials with respect to y at y = h can be represented in terms of the potential at y = h.

$$\frac{\partial U_{I,ik}}{\partial y}\bigg|_{y=h} = \kappa_{ik} \coth \kappa_{ik}h \; U_{I,ik}(y=h) \qquad (A3.32a)$$

$$\frac{\partial U_{II,ik}}{\partial y}\bigg|_{y=h} = -\kappa_{ik} \coth \kappa_{ik}d \; U_{II,ik}(y=h) \qquad (A3.32b)$$

Now, the boundary conditions, (A3.30a~c), can be solved for $[U_{I,ik}]$ and $[U_{II,ik}]$ at y = h in terms of the charge density $[\rho]$.

$$U_{I,ik}(y=h) = U_{II,ik}(y=h) = \frac{\tilde{\rho}_{ik}}{\epsilon_r \kappa_{ik}\coth\kappa_{ik}h + \kappa_{ik}\coth\kappa_{ik}d} \qquad (A3.33)$$

Then, the field values at y = h can be found by using the following relations evaluated at y = h.

$$\widetilde{E}_{x,ik}(y) = - \frac{d_{x,i}^{ND}}{\Delta x} U_{ik}(y)$$

(A3.34a)

$$\widetilde{E}_{z,ik}(y) = - \frac{d_{z,i}^{DN}}{\Delta z} U_{ik}(y)$$

(A3.34b)

From this point on, the two-dimensional field arrays are changed into the corresponding one-dimensional vectors for convenience of formulation according to the rule described in equation (A3.15). Then, the two-dimensional N_x by N_z matrix becomes an Nx*Nz column vector and the relations (A3.34a and b) can be expressed in the matrix form:

$$\begin{bmatrix} \widetilde{E}_x \\ \widetilde{E}_z \end{bmatrix} = \begin{bmatrix} [\widetilde{G}_{x\rho}] \\ [\widetilde{G}_{z\rho}] \end{bmatrix} [\widetilde{\rho}]$$

(A3.35)

where the $[G_{x\rho}]$ and $[G_{z\rho}]$ are diagonal matrices.

The final boundary condition is that the tangential electric field should be zero on the metal strip. In order to apply this condition, we have to go back to the original domain using the inverse transformation relation

$$[E_x] = ([T_z^{DN}] \otimes [T_x^{DN}]) [\widetilde{E}_x]$$

(A3.36a)

$$[E_z] = ([T_z^{ND}] \otimes [T_x^{ND}]) [\widetilde{E}_z]$$

(A3.36b)

$$[\rho] = ([T_z^{DN}] \otimes [T_x^{ND}]) [\widetilde{\rho}]$$

(A3.36c)

where $\otimes$ is the Kronecker product defined by (A3.17).

Then,

$$\begin{bmatrix} E_x \\ E_z \end{bmatrix}_{red} = \begin{bmatrix} [G_{x\rho}] \\ [G_{z\rho}] \end{bmatrix}_{red} [\rho]_{red} = [0]$$

(A3.37)

where the subscript 'red' denotes the reduced matrix obtained by deleting the rows and columns corresponding to the non-metallic discretization points. The static charge distribution can be calculated from equation (A3.37) by using the QR algorithm. After the values of the potentials, $U_{I,ik}$ and $U_{II,ik}$ at $y = h$, are found from the static charge distribution, the coefficients $A_{I,ik}$ and $A_{II,ik}$ in (A3.31a and b) can be obtained by evaluating the potential values at $y = h$, from which the electric field distributions can be calculated by equations (A3.34a and b).

Bibliograph

[1] D. S. James and S. H. Tse, "Microstrip End Effect," *Electroni. Lett.*, vol. 8, pp. 46-47, Jan. 1972.

[2] P. Silvester and P. Benedek, "Equivalent Capacitances of Microstrip Open Circuits," *IEEE Trans. Microwave Theory Tech.*, vol. MTT-20, pp. 511-516, Aug. 1972.

[3] T. Itoh, R. Mittra and R. D. Ward, "A Method for Computing Edge Capacitance of Finite and Semi-Infinite Microstrip Lines," *IEEE Trans. Microwave Theory Tech.*, pp. 847-849, Dec. 1972.

[4] C. Gupta and A. Gupinath, "Equivalent Circuit Capacitance of Microstrip Step Change in Width," *IEEE Trans. Microwave Theory Tech.*, vol MTT-25, pp. 819-822, Oct. 1977.

[5] A. F. Thomson and A. Gopinath, "Calculation of Microstrip Discontinuity Inductances," *IEEE Trans. Microwave Theory Tech.* vol. MTT-23, pp. 648-655, Aug. 1975.

[6] P. Stouten, "Equivalent Capacitances of T Junctions," *Electron. Lett.*, vol. 9 pp. 552-553, Nov. 1973.

[7] I. Wolff, A G. Kompa and R. Mehran, "Calculation Method for Microstrip Discontituities and T-Junctions," *Electron. Lett.*, vol. 8, pp. 177, Apr. 1972.

[8] P. Silvester and P. Benedek, "Microstrip Discontinuity Capacitances for Right-Angle Bends, T Juntions, and Crossings," *IEEE Trnas. Microwave Theory Tech.*, vol. MTT 21, pp. 341-346, May 1973.

[9] M. Maeda, "An Analysis of Gap in Microstrip Transmission Lines," *IEEE Trans. Microwave Theory Tech.*, vol. MTT-20, pp. 390-396, June 1972.

[10] A. Farrar and A. T. Adams, "Matrix Method for Microstrip Three-Dimensional Problems," *IEEE Trans. Microwave Theory Tech.*, vol. MTT-20, pp. 497-504, Aug. 1972.

[11] G. Kompa and R. Mehran, "Planar Waveguide Model for Calculating Microstrip Componenets," *Electron. Lett.*, vol. 11, pp.459-460, Sep. 1975.

[12] R. Mehran, "The Frequency-Dependent Scattering Matrix of Microstrip Right-Angle Bends, T-Junctions and crossings," *AEU.*, vol.29, pp. 454-460, Nov. 1975.

[13] R. H. Jansen, "The Spectral-Domain Approach for Microwave Intergrated Circuits," *IEEE Trans. Microwave Theory Tech.*, vol. MTT-33, pp. 1043-1056, Oct. 1985.

[14] T. Itoh, "Analysis of Microstrip Resonators," *IEEE Trans. Microwave Theory Tech.*, vol. MTT-22, pp. 946-952, Nov. 1974

[15] T. Uwano, R. Sorrentino and T. Itoh, "Characterization of Stripline Crossing by Transverse Resonance Analysis," 1987 IEEE Microwave Theory Tech. Symp. Digest, pp. 777-178

[16] R. Sorrentino and T. Itoh, "Transverse Resonance Analysis of Finline Discontinuities," *IEEE Trans. Microwave Theory Tech.*, vol. MTT-32, Dec. 1984.

[17] R. W. Jackson and D. M. Pozar, "Full-Wave Analysis of Microstrip Open-End and Gap Discontinuities in Millimeter-Wave Integrated Circut," *IEEE Trans. Microwave Theory Tech.*, vol. MTT 33, pp. 1036-1042, Oct. 1985.

[18] P. B. Katehi and N. G. Alexopoulos, "Frequency-Dependent Characteristics of Microstrip Discontinuities in Millimeter-Wave Integrated Circut," *IEEE Trans. Microwave Theory Tech.*, MTT-33, pp.1029-1035, Oct. 1985.

[19] K. S. Yee, "Numerical Solution of Initial Boundary Value Problems Involving Maxwell's Equations in Isotropic Media," *IEEE Trans. Antennas Propagat.*, vol. AP-14, pp. 302-307, May 1966

[20] S. Akhtarzad and P. B. Jones, "Solution of Maxwell's Equations in Three Space Dimensions and Time by T.L.M. Method of Numerical Analysis," *Proc. IEE*, vol. 122, pp. 1344-1348, Dec. 1975.

[21] G. Metzger and J. P.Vabre, "Transmission Lines with the Pulse Excitation," New York, Academic Press, 1969, pp. 65-96.

[22] N. Yoshida and I. Fukai, "Transient Analysis of a Stripline Having a Corner in Three-Dimensional Space," *IEEE Trans. Microwave Theory Tech.*, vol. MTT-32, May 1984.

[23] S. Koike, N. Yoshida and I. Fukai, "Transient Analysis of Coupling Between Crossing Lines in Three-Dimensional Space," *IEEE Trans. Microwave Theory Tech.*, vol. MTT-35, pp. 67-71, Jan. 1987.

[24] Y. C. Shih and W. J. R. Hoefer, "Dominant and Second-Order Mode Cutoff Frequencies in Fin Lines Calculated with a Two-Dimensional TLM Program," *IEEE Trans. Microwave Theory Tech.*, vol. MTT-28, pp.1443-1449, Dec. 1980.

[25] X. Zhang, J. Fang, K. K. Mei and Y. Liu, "Calculations of the Dispersive Characteristics of Microstrips by the Time-Domain Finite Difference Method," *IEEE Trans. Theory Tech.*, vol. 36, pp. 263-267, Feb. 1988.

[26] X. Zhang and K. K. Mei, "Time-Domain Finite Difference Approach to the Calculation of the Frequency-Dependent Characteristics of Microstrip Discontinuities," *IEEE Trans. Microwave Theory Tech.*, vol.36, pp. 1175-111787, Dec. 1988.

[27] W. F. Ames, "Numerical Methods for Partial Differential Equations," Academic Press, New York 1977, pp. 302-304.

[28] A. Taflove and K. R. Umashanker, "The Finite-Difference Time-Domain Method for Electromagnetic Scattering and Interaction Problems," JEWA., vol. 1, No. 3, pp. 243-267, 1987.

[29] S. Nam, S. El-Ghazaly, H. Ling and T. Itoh, "Time-Domain Method of Lines Applied to a Partially Filled Waveguide," 1988 IEEE Trans. MTT-S Digest, pp. 627-630.

[30] U. Schulz and R. Pregla, "A New Technique for the Analysis of the Dispersion Characteristics of Planar Waveguides," *AEU*, Band 34, pp.169-173, 1980.

[31] S. B. Worm and R. Pregla, "Hybrid-Mode Analysis of Arbitrarily Shaped Planar Microwave Structures by the Method of Lines," *IEEE Trans. Microwave Theory Tech.*, vol. MTT-32, pp. 191-196, Feb. 1984.

[32] S. Nam, H. Ling and T. Itoh, "Time-Domain Method of Lines Applied to Finned Waveguide," 18th European Microwave Conference Procedings, PP.1095-1099, 1988.

[33] H. Diestel and S. B. Worm, "Analysis of Hybrid Field Problems by the Method of Lines with Nonequidistant Discretization," *IEEE Trans. Microwave Theory Tech.*, vol. MTT-32, pp.633-638, June 1984.

[34] R. E. Collin, "Field Theory of Guided Waves," McGraw-Hill Book Company, New York 1960, pp. 483-485.

[35] S. Nam, H. Ling and T. Itoh, "Time-Domain Method of Lines Applied to the Uniform Microstrip Line and its Step Discontinuity," to be presented at 1989 IEEE MTT International Symposium, Long Beach CA, June 1989.

[36] K. C. Gupta, R. Garg and I. J. Bahl, "Microstrip Lines and Slotlines," Artech House, Inc.,1979.

[37] D. L. Gish and O. Graham, "Characteristic Impedance and Phase Velocity of a Dielectric-Supported Air Strip Transmission Line with Side Wall," *IEEE Trans. Microwave Theory Tech.*, vol. MTT-18, Mar. 1970.

[38] C. H. Chan, K. T. Ng and A. B. Kouki, "Propagation Characteristic for a Suspended Substrate Microstrip Line with Pedestal," Submitted for Publication in IEEE Microwave Theory Tech.

[39] W. L. Stutzman and G. A. Thiele, "Antenna Theory and Design," John Wiley & Son, Inc., pp. 87-91, 1981.

[40] "The IMSL Library," IMSL, Inc., Edition 9.2, subroutine LLSQF, 1984.